# Functionalized Bead Based Microchip for Immunoassay and Virus Immuno-affinity Chromatography

by

Le Zhang

A thesis submitted in partial fulfillment of the requirements for the degree of

Master of Science

Department of Chemistry
University of Alberta

# Abstract

We demonstrate the functionalization of a highly ordered porous molecular sieving matrix created by colloidal self-assembly (CSA) of 2 micrometer diameter silica particles in microfluidic chips, for highly efficient immuno-capture of viruses. By tuning the particle size, with appropriate surface chemistry, we can easily match the pore size which could maximize biological species-particle wall collision, leading to highly capture efficiency. The ordered uniform lattice of pores, which provides 15 % the size of the particles used, should prove ideal for the capture of viruses (on the 50-150 nm scale in size). We report on characterization of capture beds with 300 nm pores using fluorescein and anti-fluorescein, and the application to capture and detection of suspensions of type-5 adenoviruses, and of same virus in infected cells. We demonstrate the performance of the concept using a fully packed column for fluorescein immunoassay. We used 2 μm carboxylated silica particles self-assembled into a 6 mm long-bed, modified with EDC/NHS, and immobilized anti-fluorescein antibody or type-5 adenovirus-recognizing antibody. An electric field was applied to utilize electro-osmotic flow as the solvent pumping force. A 4.51 nM fluorescein solution was captured by immuno-affinity using anti-fluorescein antibody, and then released with an eluent to an empty downstream analysis region to give a very large signal, providing a positive control. Similar experiments were performed with type-5 adenovirus, demonstrating detection at a concentration of $8.3 \times 10^3$ viral particles (VP) per milliliter. Adenovirus in cell

lysate was also detected in this microchip, with the lowest concentration detectable at $1.5 \times 10^3$ PFU/mL. Combination of advanced biological detection methods with microfluidics based extraction and concentration techniques has tremendous potential for realization of a portable, cost effective and sensitive pathogen detection system. Taking advantage of the unique fluid flow characteristics of CSA structures on an even smaller scale than employed here, faster, more sensitive and more economical capture and pre-concentration techniques for diagnostic assays for a wider range of analytes can be developed.

# Preface

None of this thesis has been previously published.

# Acknowledgement

I'd like to start my thesis with all my sincerest gratitude to Dr. D. Jed Harrison, my research supervisor during my stay in Department of Chemistry in University of Alberta. His brilliance and insights towards the research enlightened my way and his enthusiasm for challenge and success in life deeply inspired me.

I could not count how many times I have felt so lucky that Dr. Harrison took me into his group, one of the world's pioneers in microfluidic technology. I thank him for showing me how interesting microchip technology is. I thank him for giving me directions with great patience whenever I felt lost during my research. I also thank him for providing me the great opportunity to attend the EnviroAnalysis Conference 2013 in Toronto City where I could gain more insights and present my work in public.

I also want to thank Dr. Mark T. McDermott and Dr. Jilian M. Buriak for being my supervisory committee members. Together with Jed, their guidance kept me in the right path.

I also want to thank Dr. Abebaw Jemere, a good mentor in DJH group to me and a very good friend, who shared his spectacular research experiences and who helped me with some experimental design. His brilliance and patience made all things easier for me.

I also appreciate all the help from our DJH group members, my lovely lab mates who made our lab a great place to rock and roll. I want to thank the support from

Karen Mckinley, Sharlene Oliver, Dr. Eric Flaim, Dr. Wenming Ye, Huiying Sheng, Dr. Sabrina Peng, Dr. Yongxin Zhao, Dr. Amr Mohamed, Dr. Donghai Lin, Narges Shabani, Hamid Ramezani, Ya Zhou, Yufeng Zhao, Jing Ji, and lastly my very good friends Mohammed Azim, Dr. Mirza Galib and Dr. Reshma Singh. Thank you all for making U of A the greatest experience in my life.

I thank all the help from the support staffs in electronic shop, general office, machine shop, SEM and Nanofab. I also want to thank some special best Chinese friends who made my life in Edmonton enjoyable: Jing Liu, Yue Wu, Lei Wang, Sharon Chen, Fenglin Liu, Bing Cao, Jing Li, Jingjing Zhang.

At last, I want to give my deepest gratitude to my parents and siblings who gave their best to support me. Thanks for the selfless love they are giving and thanks for always being there when nobody was.

# Table of Contents

## Chapter 1 Introduction



## Chapter 2 Functionalized bead based porous structure in microchip for immunoassay and immuno-affinity chromatography

## Chapter 3 Conclusions and future work

# List of Tables

# List of Figures

## Chapter 1



## Chapter 2

# List of Abbreviations

| | |
|---|---|
| cfu | Colony forming unit |
| CSA | Colloidal self-assembly |
| CTC | Circulating tumor cell |
| DMF | Digital microfluidic |
| EDL | Electrical double layer |
| ELISA | Enzyme Linked Immunosorbent Assay |
| EOF | Electrokinetic flow |
| GEDI | Geometrically enhanced differential immunocapture |
| IVD | In vitro-diagnostics |
| LoC | Lab-on-a-chip |
| MEMS | Microelectromechanical systems |
| PCR | Polymerase chain reaction |
| PDMS | Poly (dimethylsiloxane) |
| PFU | Plaque forming unit |
| POC | Point-of-care |
| qPCR | Quantitative real-time PCR |
| RT-PCR | Reverse transcription polymerase chain reaction |
| SEM | Scanning electron microscopy |
| VP | Viral particles |
| μTAS | Miniaturized total analysis systems |

# Chapter 1 Introduction

## 1.1 Microfluidic and its application for pathogen detection

Microfluidic systems are a key component of miniaturized total analysis systems (μTAS)[1,2] or Lab-on-a-chip (LoC) technologies. By manipulating small amounts of sample fluid in a confined micro-channel, μTAS device can be applied to research areas in chemistry and biochemistry. The first demonstration of microfluidic technologies was accomplished for separation studies. These devices offered several useful characteristics, such as using a small amount of sample, high resolution, and a short time for analysis.[3] A real stimulus for the rapid growth of academic research in microfluidics arose from a series of programs supported by the US Department of Defense in the 1990s. These programs aimed at developing field deployable microfluidic based detectors for chemical and biological threats posed by militaries and terrorists.[4] The great success of photolithography and its associated technologies in silicon microelectronics and microelectromechanical systems (MEMS) have made a major contribution to the development of a first generation of silicon LoC technologies[4], which can be directly applied to microfluidics. Silicon, however, has been gradually replaced by other materials such as poly (dimethylsiloxane) (PDMS)[5], which is more biocompatible, and exhibits electroosmotic flow (EOF). PDMS is a supporting material that can be rapidly fabricated at a low cost, and offers simplicity for integrating membrane based pumps and valves.

Due to the obvious advantages over conventional macro-scale methods, a very important goal of microfluidic scientists is to develop novel approaches to demonstrate the efficiency of this new technology in biology and biomedical research[6], especially in diagnosis. Over a decade ago, people wrote that "microfluidics has the potential to significantly change the way modern biology is performed." [6,7] The global in vitro-diagnostics (IVD) market is close to $44 billion in 2011, doubled from what it was in 2001 and will keep continue growing.[8] The size of this market creates interest in microfluidic based diagnostic systems which are rapid, cost effective and user friendly, as they are believed to be the perfect candidates for point-of-care devices. Researchers continue to work to make this tool a reality. Microfluidics offers a high surface to volume ratio and a faster mass and heat transfer rate. Furthermore, the ability to handle nano to picoliters of fluid sample is an important prerequisite for a cost effective device.[9] The potential integration of microfluidic with other functions such as valves, pumps, mixers and detectors could lead to the goal of increased point-of-care (POC)[10] devices in the market place.

Microfluidic based immunoassays can be used to detect various target analytes such as pathogens in human blood or food, and also biomarkers for cancers. According to a recent report from The World Health Organization (WHO)[9], infectious diseases, which are often detected by immunoassay, are the second leading cause of mortality throughout the world, next to cardiovascular disease.

More than half of these deaths in developing countries occur due to a low level of hygiene and limited access to well-equipped labs for diagnostics and treatments of infectious disease.[11-13] The situation can be changed by diagnosing the pathogen in a very early stage, which can greatly increase the chance of disease control, such as at the early stage of epidemic, and foodborne pathogens tracing. In developed countries, there are still problems that remain to be resolved. These include food safety issues, sexually communicative diseases and cancers, despite the great progress in the enhancement of health conditions.[14] People believe that the metastases in patients with solid tumor malignancy are developed from the tumor cells that move into the circulation system and migrate to distant organs, extravasate and then multiply.[15-18] As a tumor develops, the cells or the organ releases specific proteins called biomarkers and the levels of these biomarkers in the human circulation system are directly related to the stages of the tumor.[19] Identification and isolation of these biomarkers are therefore of great use for clinically monitoring the patients and immunoassays are often used.

Immunoassays have been applied to quantitatively determine target molecules in many applications, such as clinical diagnostics, proteomics and pharmaceutical research. Immunoassays are also commonly used in clinical quantitative biomarkers detection, due to the highly specific molecular antibody-antigen epitope recognition.[10,20-22] Immunoassays can be classified into two different

categories based on the antibody and antigen interaction. Heterogeneous immunoassays allow antigen interactions with antibody immobilized on a solid support, while in homogenous immunoassays, the interaction happens in solution. Labels on a secondary antibody that recognizes the antigen when complexed with the primary antibody are the most significant for signal transduction and amplification. Fluorescent substrates, enzymes, redox molecules and quantum dots are utilized for immuno-sensing labels.

The identification of DNA/RNA in the pathogen often requires cell culture, and, due to the low-concentration of genetic materials in the sample. This technique often requires amplification such as traditional polymerase chain reaction (PCR), which involves delicate sample preparation and highly trained personnel to perform.

Label-free immunoassay and quantitative real-time PCR (qPCR) techniques can provide both sensitive and multiplexing detection at clinically relevant levels, to diagnose disease at an early stage. However, these conventional pathogen detection techniques usually requires long preparation processing time, may require a significant sample amount, and certainly need qualified personnel. Compared to these traditional methods, a microfluidic system that is fast and sensitive may be a better alternative platform technology for rapid, portable diagnosis[23], though trained personnel may still be required. Also, the ability to

perform multiplexing in one device is another significant characteristic for microfluidic device in cases when diseases are caused by several pathogens.[11] Past achievements with integrating traditional technologies onto a chip have enabled many possibilities. D. S. Reichmuth et al.[24] developed a microfluidic device that integrated a nano-porous polyacrylamide membrane within the micro-channel to electrophoretically concentrate the sample, then used fluorescence as the signal for swine influenza virus detection. The total assay requires less than a 50 μL sample, and works within 6 minutes. X.A. Guan et al. [25] demonstrated an immuno-separation platform that utilized antibody functionalized glass beads based for micro-organism detection. Concentration of E. coli was used as a model of the analyte; the signal was collected by detecting ATP bioluminescence reaction on chip. This chip showed excellent specificity and reproducibility for E. coli O157: H7 in the range of $3.2 \times 10^1$ cfu/μL to $3.2 \times 10^5$ cfu/μL within 20 minutes. Y. Li et al.[26] reported a device that integrated reverse transcription polymerase chain reaction (RT-PCR) with online fluorescence detection and realized a rapid pathogen detection system that performs both genetic amplification and product analysis. This device successfully amplified and detected rotavirus from stool sample with a RNA detection limit of $3.6 \times 10^4$ copies $\mu L^{-1}$ within an hour of operation.

Silicon and glass were used as the substrate for the first generation of microfluidics, in which photolithography and wet-etching and other

microfabrication techniques were used to achieve the micro-channels.[3,27] Later, poly (dimethylsiloxane) (PDMS) emerged as a commonly used alternative material to silicon and glass, due to its simple fabrication process, flexibility, optical transparency, biocompatibility and low autofluorescence properties, and simplicity of bonding to glass and silicon.[28,29] New materials such as paper[30-34] and cotton thread[35] have also been developed for simple and low cost platform for point-of-care diagnosis.

### 1.2 Amplification and pre-concentration techniques

Pathogen detection is usually achieved based on two aspects: by identification of specific epitopes on the pathogen surface using antibody or alternatives, or by recognition of the genetic information. Nucleic acid based techniques usually provide a better specificity, but a lower efficiency, due to the more tedious sample preparation process. The often low concentration of pathogen genetic material in a sample matrix is another challenge for detection; thus an amplification mechanism is usually necessary in developing an effective biosensor. For nucleic acid based techniques, polymerase chain reaction (PCR) is the most widely used amplification tool. For antibody-antigen based detection, the surface capacity and interaction between the antibody and antigen directly influence the immunoassay quality. So, in order to increase the surface capacity and also maximize the analyte-wall interaction, nano-porous structures or posts structure have been fabricated and integrated into the diagnostic systems.

### 1.2.1 PCR

PCR is a technique that can exponentially increase the target DNA or RNA molecules through controlling the thermal cycling. A typical cycle includes denaturing, annealing, and then extension. PCR was first introduced by Mullis and co-workers[36] in 1985. They described the successful transition of a mixture of bacterial polymerase, dNTPs, template DNA, and primers into exponentially increased pieces of template DNA by controlling the thermal energy. Mullis was awarded the Nobel Prize in chemistry in 1993 for this work. Now that the human genome discovery era is over, genetic information plays a significant role in discovering genetically related health issues and diseases, and PCR is a necessity to create adequate copies of DNA sequences for study. Over the years, people have developed similar techniques based on conventional PCR for different applications, such as quantitative real-time PCR (qPCR), and reverse transcription quantitative PCR (RT-qPCR). Utilizing a fluorescence detector and engineering fluorescence emission by PCR products, real time monitoring of the DNA copy amplification can be recorded. Cheng et al.[37], McGuinness et al.[38], and Hein et al.[39] utilized qPCR to detect Salmonella spp., a foodborne pathogen in artificial contaminated meat, potatoes and other food samples. Rodriguez-Manzano et al.[40] used qPCR to detect Hepatitis A virus in a raw sewage water sample.

Despite the advantages of highly sensitive detection of pathogens, conventional PCR techniques suffer from high cost per sample, and easy sample contamination. Recently, combinations of PCR[41-43] and qPCR[44,45] with microfluidics have been demonstrated. This approach offers a faster reaction time, due to a smaller thermal mass, consumes less reagent, and has the possibility of integration of other functional tools for subsequent analysis. Of techniques that have been reported, PCR using digital microfluidic (DMF) devices which manipulate (moving, merging, mixing, splitting, and dispensing from reservoirs) droplet samples, offering precise control over several reagent phases, has been successfully commercialized. The initial complete implementation of PCR into DMF was reported by Chang et al.[46] The fluorescence signals generated from this device were comparable to a bench-scale PCR instrument, with 50% and 70% reductions in total time and sample consumption.[47] Expanded work that performs real-time PCR[48] or multiplexed real time PCR[49] has been reported. PCR remains a complex laboratory technique that requires good quality control and well trained personnel.

### 1.2.2 Nano-porous structure/membrane

For an immunosorbent assay based on an antibody-antigen interaction, surface capacity and interaction efficiency are directly related to the quality of assay. Microfluidic devices demonstrate great potential for advances in integrating nano-porous material or structure for immunoassay pre-concentration. With high

surface area, the tunable geometries of microfluidic systems offer a length scale that can match the analyte size, which conceptually would provide a maximum cell-wall collision with a wide range of surface functionalization available for integration.[50] Recently, micro-posts structures modified with antibody in microfluidic devices have been successfully used for circulating tumor cell (CTC) capture. The concept can be extended to other analytes and sizes, which is the subject of this thesis.

Capturing and enumerating specific cells in humans or animals is a significant long standing field, due to the potential application in implementing diagnostic and prognostic testing for diseases, tumors, inflammatory responses or hematological information.[51-53] By functionalizing a surface with antibodies, proteins or aptamers that can specifically bind to cell surfaces, target cells can be captured and counted from complex samples.[51] The portability, low cost and sensitivity are also important factors for evaluating the usefulness of a system. In the case of circulating tumor cells, by optimizing the system with both chemical and fluid-dynamics, the efficiency of rare cell isolation can be greatly improved.[54] X. Cheng et al.[55] developed a microfluidic device which was implemented with cell affinity chromatography, operated under differential shear flow, to specifically isolate CD4+ T lymphocytes from unprocessed, unlabelled whole blood. Cell counting was achieved using an optical microscope; rapidly and simply. S. Nagrath et al.[56] described a unique microfluidic design which can

efficiently and selectively separate circulating tumor cells (CTC) in the blood by mediating the interaction of target CTCs with antibody coated micro-posts with precisely controlled laminar flow. This work successfully identified CTCs in patients' blood samples with metastatic lung, prostate, pancreatic, breast and colon cancer. A. H. Talasaz et al.[57] demonstrated a novel immuno-magnetic cell separator which could enrich target cells and eliminates cells that are non-binding or non-specifically binding. The system has the ability to process a 9 mL blood sample with a capture efficiency of over 50% for circulating epithelial cells (CEpCs). B. J. Kirby et al.[15] developed a geometrically enhanced differential immunocapture (GEDI) microfluidic device which combines an antibody functionalized 3D geometry that captures circulating tumor cells. The sensitivity improved 2-400 fold compared to the commercially available CellSearch® system. GEDI was an improvement over the work of Toner[58], which also used micro-posts for collisions, in that Kirby optimized collision frequency by manipulating the axis of the post lattice structure, as in Figure 1-1. The GEDI device is a notable improvement because the enhanced collision frequency greatly reduced the time required for the same amount of sample to collide with the posts walls.

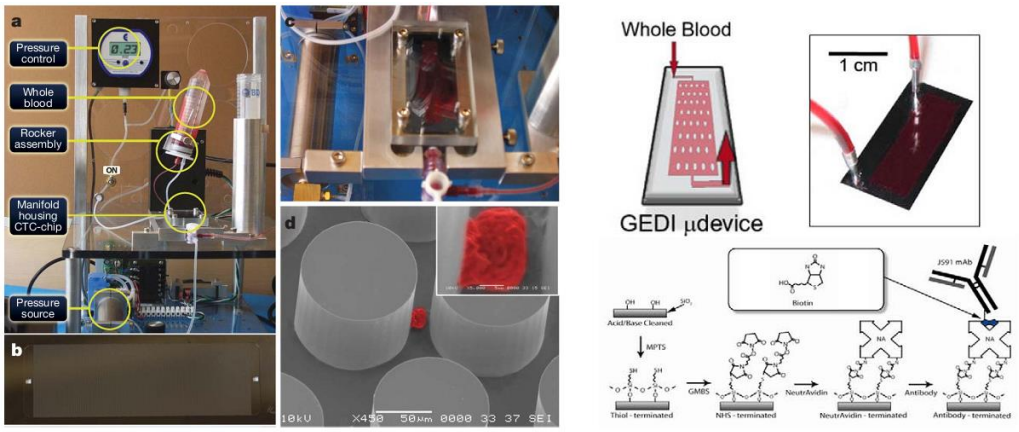


Figure 1-1. (A) Isolation of CTCs from whole blood using a microfluidic device. **a**, The workstation setup for CTC separation. The sample is continually mixed on a rocker, and pumped through the chip using a pneumatic pressure-regulated pump. **b**, The CTC-chip with micro-posts etched in silicon. **c**, Whole blood flowing through the microfluidic device. **d**, Scanning electron microscope image of a captured NCI-H1650 lung cancer cell spiked into blood (pseudo coloured red). The inset shows a high magnification view of the cell.[56, §] (B).GEDI device overview. Clockwise from upper left: schematic of blood flow through device, image of silicon device with silicone gasket, surface functionalization scheme.[15, þ]

---

§ Copyright by Nature Publication Group, used with permission.

þ Open source by PLOS ONE

CTC sorting and capturing by immunoassay in the GEDI device is a real achievement toward clinical diagnosis of patient's tumor development. However, capturing CTC's is not the only way to perform cancer monitoring. Biomarkers released into the human circulation system, which are related to the stage of the tumor, present an alternative route for evaluation. Also, besides diagnosing tumors, pathogen detection in the food industry, water supplies, the environment, clinical diagnosis, and national defense are all of great interest, and have potential impact on society. The GEDI is a size dependent device that fractionates CTC from a matrix sample and has high efficiency, due to the delicate fabricated posts within the micro-channel. However, the scale of cells is in the 1-30 μm range, and post fabrication below this range requires nanolithography and is very expensive. A typical virus size (20-100 nm) is usually 10 or more times smaller than a CTC.[59] Facile fabrication of smaller pore sizes can be achieved by three dimensional colloidal self-assembly (CSA) within a micro-channel.[60] Fabrication of GEDI-like architectures by CSA, using various particles sizes, allows real flexibility and could lead to low cost for the capture and analysis of virus particles.

Spontaneous organization of monodispersed micro or nanoparticles is termed colloidal self-assembly (CSA)[60]. CSA has been used in material synthesis[61], photonic band gap crystals[62], and biochemical sensors.[63] Colloidal self-assembly (CSA) in microfluidic devices was developed by the Harrison group for

biomolecular separation.[60] They utilized silica or polystyrene nano/micro particles to form an ordered three dimensional porous structure for molecular sieving, and have shown its use for protein[60] and DNA separation.[64-66] Figure 1-2 shows the fabrication process of CSA in micro-channels and its preliminary application for protein separation. Evaporation induced colloidal self-assembly forms a highly ordered sieving structure for biomolecules, which could potentially lead to high efficiency on-chip bioseparations. Figure 1-3 shows the application of CSA in protein and DNA separation as applied by the Harrison group. In their work, buffers have been used to minimize the analyte-particle interaction. The hexagonal close packed lattice formed by CSA creates a lattice of pores with a highly tortuous pathway that will lead to frequent collision between analytes and particle surfaces. We reason that by modifying the particle surface with specific recognition reagents, CSA might have application in diagnosis as an efficient capture matrix.

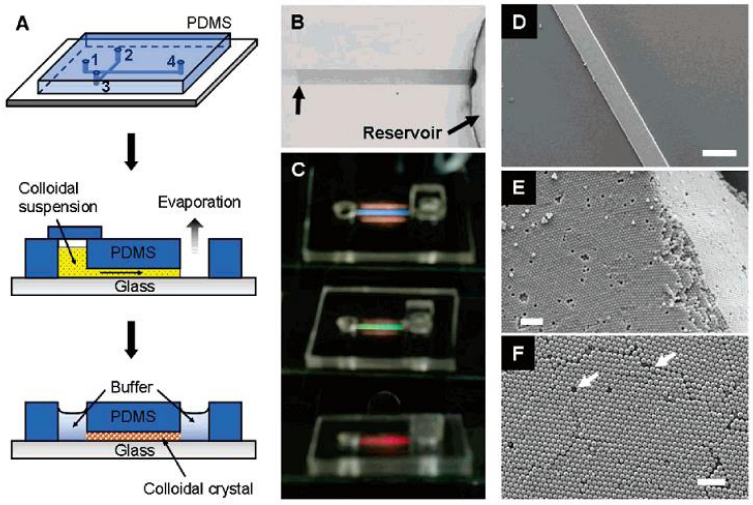


Figure 1-2. Fabrication and characterization of self-assembled colloidal arrays within microfluidic systems. (A) Schematic illustration of microfluidic colloidal self-assembly in a one-dimensional separation microchip (PDMS chip layout: 1 buffer, 2 sample, 3 sample waster, 4 buffer waste). (B) Optical micrograph of a translucent 0.9-μm silica sphere array growing inside a micro-channel (as indicated by the left arrow), showing a convex evaporation interface at the channel opening. (C) Digital images of a PDMS chip packed with 0.9-μm silica spheres before drying. When illuminated by white light vertically from the bottom, the array exhibited monochromic transmitted light at various angles due to Bragg diffraction. (D, E) SEM images of a matrix of 330-nm silica spheres at different magnifications. (F) SEM image of a hexagonally closed packed 2-μm PS colloidal array fabricated within a microchannel. The arrows indicate lattice defects. The scale bars are 200, 2, and 10 μm (D-F), respectively.[60, ς]

---

ς Copyright by American Chemical Society, used with permission.

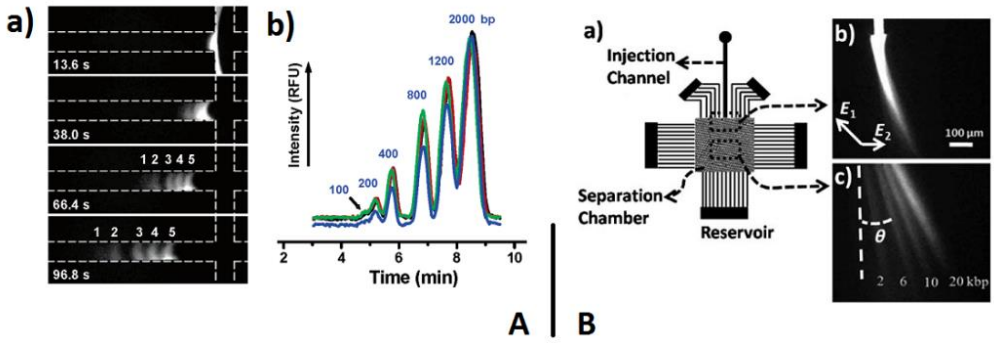


Figure 1-3. A. (a) Sequence of fluorescent images of the electrophoretic separation (15 V/cm) of a low DNA mass ladder in a microfluidic chip packed with 0.9-μm silica beads. In this case, the microchip has ~ 100-μm-wide and ~ 20-μm-deep microchannels with a cross-injection design. Frames are time-stamped in seconds. DNA fragments 1-5 are assigned as 200, 400, 800, 1200, and 2000 bp, respectively. (b) Four consecutive runs of the same ladder obtained using 0.9-μm silica beads in a device that had been operated for ~5 h (E) 19.2 V/cm, separation length L= 5 mm).[60,3] B. a) Schematic and b, c) photomicrographs of the DNA separation microchip used in this work. DNA solution is injected continuously into the separation chamber. White arrows represent the directions of the applied electric fields (b). The separation chamber is filled with nanoparticle arrays. Different sizes of DNA molecules separate from each other and form individual streams, each deflecting an angle $\theta$ from the injection angle (c).[64, 2]

---

[3] Copyright by American Chemical Society, used with permission.

[2] Copy right by John Wiley and Sons, used with permission.

### 1.3 Fluid manipulating forces

Microfluidic devices are designed to perform sample introduction, mixing, reaction, dispensing, separation and detection through different regions of the micro-channels.[67] Mixing is the key part for successful immunoassays. Forces are required for fluid sample manipulation within microfluidic systems, which usually can be divided into pressure driven and electrokinetically driven. Syringe pumps have been used to deliver fluid by external connections. Other varieties of micropumps have been recently developed to be seamlessly embedded into a microchip platform. B.D Iverson et al.[68] reviewed and evaluated the most recent micropump advances. References can be found under each category and will not be discussed here. The pumps discussed in the review include piezoelectric[69-76], electrostatic[77,78], electromagnetic/magnetic[79,80], thermal[81,82], pneumatic[83,84], composite/polymer materials[84,85], irreversible[75,86], peristaltic[87,88], valves[89], ferrofluid[90], phase change[91,92], gas boundary[93,94], rotating gear[95,96], viscous Force[97,98], induction[99,100], injection[101,102], polarization[103], ion drag[104], DC electroosmotic[105], AC electroosmotic[106,107], magnetohydrodynamic[108], electrowetting[109,110], optoelectrostatic microvortex[111], flexural plate wave.[112] An immense amount of successful and notable pressure driven based microfluidic systems for immunoassay have been achieved. One method of particular interest was accomplished by C.D. Chin et al.[113] using a syringe induced vacuum as the driving force, as shown in Figure 1-4. The so called 'mChip' showed good performance for HIV and syphilis detection in Rwanda, rivaling reference bench

top assays. Despite all the advantages, integration of micro pumps still faces challenges such as higher cost and complexity.

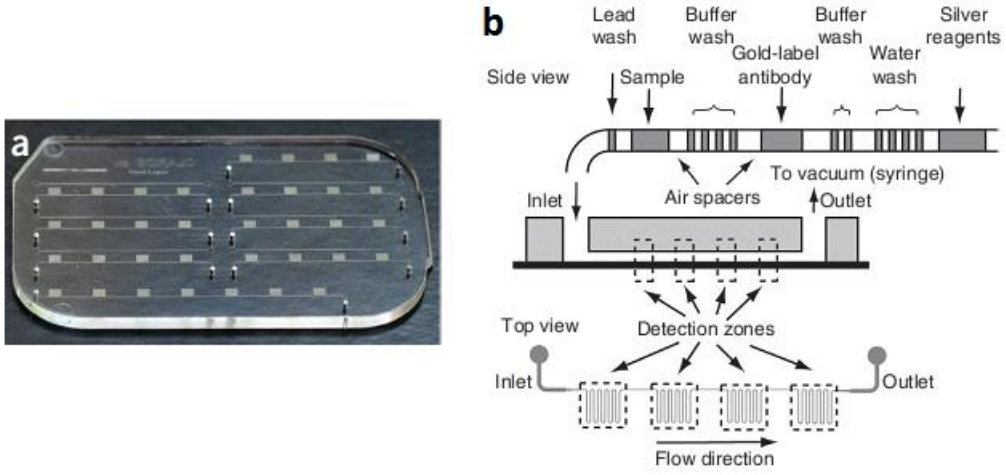


Figure 1-4. Schematic diagram and pictures of microfluidic device, and data on fluid handling of a POC ELISA-like assay. (a) Picture of microfluidic chip. Each chip can accommodate seven samples (one per channel), with molded holes for coupling of reagent-loaded tubes. (b) Schematic diagram of passive delivery of multiple reagents, which requires no moving parts on-chip. A preloaded sequence of reagents passes over a series of four detection zones, each characterized by dense meanders coated with capture proteins, before exiting the chip to a disposable syringe used to generate a vacuum for fluid actuation.[114, ξ]

---

[ξ] Copyright by Nature Publishing Group, used with permission.

Electrokinetic flow usually involves using an external electric field to generate the movement of ions in the solvent, as well as motion of the solvent. Unlike micropumps, which are usually based on mechanical displacement involving using a rotating gear or diaphragm to generate a pressure difference to move the fluid sample, electrokinetically driven systems offer a continuous, constant and steady flow. Electrokinetically driven flow usually refers to electroosmosis and electrophoresis. Electrophoresis will not be discussed here.

Electroosmotic flow (EOF) is the bulk movement of an aqueous solution along a stationary solid surface, which has an electrical double layer (EDL) as illustrated in Figure 1-5.[115] The flow results from applying an electric field in the presence of free ions and the charged surface at the solid-liquid interface. The surface charge attracts counterions from solutions creating an electric double layer at the interface. The field parallel to the surface mobilizes anions to the anode and cations to the cathode. Since the negative surface is immobile, this creates a flow if cations and solvent in the double layer towards the anode. In the solution bulk, the motion of anions and cations cancel each other, so only the double layer region outside the plane of shear (Figure 1-5) creates the electroosmotic flow. Viscosity and laminar flow effects then generate a plug flow of solvent in the bulk of the fluid. The mobility of EOF can be expressed as (1):

$$\mu_{\mathrm{EOF}} = -\frac{\epsilon\zeta}{\eta} \tag{1}$$

While the velocity of EOF can be expressed as:[116]

$$v_{\mathrm{EOF}} = -\frac{\epsilon\zeta}{\eta}E \qquad (2)$$

Where $\epsilon$ is the dielectric constant, $\eta$ is the solution viscosity, $\zeta$ is the zeta potential and E is the electric field strength. The solution ionic strength and the surface charge have a profound influence on the zeta potential. Consequently, EOF is always strongly dependent on these two parameters.

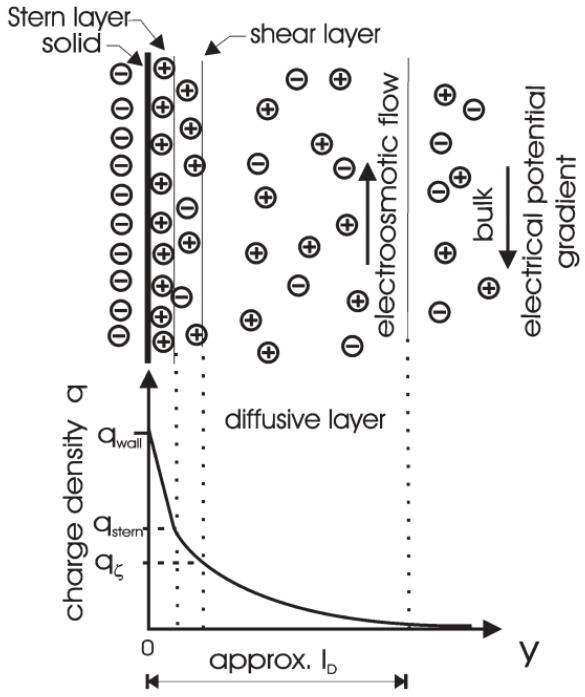


Figure 1-5. Schematic drawing of the electrical double layer and the associated charge density distribution[115, 6].

[6] Copyright by Royal Society of Chemistry, used with permission.

## 1.4 Detection methods

Fluorescence for biomolecular sensing in microfluidic systems is the most widely used and promising detection technique, due to its high sensitivity, selectivity and well-established labeling procedures. Organic dyes or other fluorophores labeled on the analytes are excited by a laser with emission detected by a photodetector. Common fluorophores used in microfluidic system include fluorescein isothiocyanate[117], Cy5[118], tetramethylrhodamine isothiocyanate (TRITC)[119], alexafluor 633.[120] Besides organic dyes, other labels such as quantum dots (QDs) have also been developed for biosensing application. QDs offer superior light stability and higher quantum yield than traditional fluorophores but the synthesis and functionalization are relatively complicated and costly. Substantial work using fluorescence detection in microfluidics for biosensing has been performed and can be found in these references.[121-125]

Besides fluorescence detection, there are other techniques that have been developed, such as luminescence, absorbance, surface plasmon resonance (SPR), electrochemical detection, and mechanical immunosensors such as micro-cantilevers. Extensive reviews on the detection methods in microfluidic systems have been done by K.N. Han et al.[10], which will not be discussed in this thesis.

## 1.5 Thesis scope and outline

This thesis presents experimental studies of functionalized colloidal self-assembly (CSA) of 2 micron silica particles in microfluidic chips for highly efficient capturing of type5-adenoviruses. The ordered uniform lattice of pores provided are 15 % the size of the particles, and should prove ideal for the capturing of viruses on the 50-150 nm scale in size. CSA in microfluidic systems was first developed by Yong and Harrison for separations.

In chapter 2, we report on characterization of the capture beds with 300 nm pores using fluorescein and anti-fluorescein, and the application to capture and detection of suspensions of type-5 adenoviruses, and of the same virus in infected cells. Using 2 μm carboxylated silica particles self-assembled into the microchip, modified with EDC/NHS, we immobilized anti-fluorescein antibody or type-5 adenovirus-recognizing antibody. We used an electric field applied to utilize electro-osmotic flow as the solution pumping force. We demonstrated immunoassay using fluorescein and anti-fluorescein antibody with a 10 mm fully packed CSA column. Then a partially packed column with 6 mm packed bed was used to perform immuno-affinity chromatography. A 4.51 nM fluorescein solution was captured by immuno-affinity using anti-fluorescein antibody, and then released with an eluent to an empty downstream analysis region to give a very large signal, providing a positive control. Similar experiments were performed with type-5 adenovirus, demonstrating detection at a concentration of

$8.3 \times 10^3$ viral particles (VP) per milliliter. Adenovirus in cell lysate was also detected in this microchip, with the lowest concentration detectable at $1.5 \times 10^3$ PFU/mL.

In chapter 3 we summarize the progress and discuss future perspectives and possibilities.

# Chapter 2 Functionalized bead based porous structure in microchip for immunoassay and immuno-affinity chromatography

## 2.1 Introduction

Immunoassay using antibody-antigen specific interaction has proven to be a very powerful tool for pathogen detection, due to the high specific recognition[126]. The analyte category can be further extended to proteins such as biomarkers for cancer diagnosis, metabolites such as glucose for diabetes monitoring, etc. However, the 96 well plate process used to perform enzyme linked immunosorbent assay (ELISA) is reagent and labor consuming and the sensitivity is not always enough to screen for early-stage infection[19]. Microfluidic based molecular diagnostic devices have evolved into a very common and successful tool for clinical diagnostics, demonstrating accuracy and efficiency over the last decades. The tremendous interest in microfluidics over traditional immunoassay is because of its small sample consumption, and fast analysis speed for pathogen detection. High sensitivity is also a key characteristic in clinical pathogen detection, due to the low concentration of many analytes. A vast amount of effort to integrate pre-concentration methods into microfluidic devices has been made. One approach of particular interest was

developed by J. T. Connelly et al.[127] They integrated nano-porous membranes in glass micro-channels as the pre-concentration method for feline calivivirus (FCV) detection in environmental water samples and used liposomes as the amplification tool. The concentrated complexes were eluted to a downstream analysis region where captured liposomes were lysed to release fluorescent molecules. Quantitative detection was achieved by image processing fluorescence from these dye molecules. The detection limit was reported to be $1.6 \times 10^5$ PFU/mL.

The structure and geometry of the substrate used for capture is certainly of significance in designing highly efficient immunosorbent assays. Functionalized posts or bead based porous structures in microfluidic chips are very promising techniques to generate high surface areas for analyte capture in next generation immunoassays. Antibody functionalized posts have been used for capturing circulating tumor cells (CTC). A very successful use of posts based on microfluidic devices for CTC capturing was accomplished by Toner and coworkers[56], in which they demonstrated a higher CTC capture efficiency than the commercialized CellSearch® systems. Kirby and colleagues[15] later developed a geometrically enhanced differential immunocapture (GEDI) microfluidic device based on this idea, which further improved collision frequencies for enhanced size dependent capture of rare circulating tumor cells.

The GEDI device for CTC capturing is a big step toward clinical diagnostics of patient's tumor development. However, infectious diseases can involve smaller pathogens such as bacteria, viruses and molecular toxins. A typical CTC is usually 10 times or more larger than a virus (20-100 nm). It is much more challenging for device fabrication on this smaller scale.

Antibody immobilization in an appropriate fashion is the most crucial step for immunosorbent assays in a microchip to be successful. Microfluidic immunoassay system using coated nanoparticles such as magnetic nanoparticles[128-130] or nanoporous membranes[131,132] and other nanostructures have great potential for efficiently improving the capture efficiency, which essentially increases the sensitivity. Recently, hydrogels providing a 3D scaffold for antibody immobilization and target capture have also been utilized for immunoassays in microfluidics.[133-136] Growth and integration of hydrogels and membranes in the micro-channel are certainly interesting; however, they usually face practical integration issues and give non-uniform pores, with variable mechanical stability.

Three dimensional colloidal self-assembly (CSA), however, could be used to fabricate very small pores using different sizes of functionalized particles within micro-channels, providing a robust, uniform porous structure with large surface binding area. CSA in microfluidic devices was developed by the Harrison group

for protein and DNA separation.[60,64,65] Binary opal lattice structure using two different sizes particles self-assemble into micro-channel for smaller pores was also fabricated by the same group and been successfully used for protein separation.[137] This device uses nano/micro particle to form a uniform 3D porous structure. The large surface to volume ratio provided is potentially useful to increase the sensitivity.

We here present the usage of CSA in a microfluidic device to perform immunoassay on fluorescein and size based immnuo-affinity chromatography for virus capture. We first performed immunoassay using fluorescein and anti-fluorescein antibody with a fully packed CSA column. Then a partially packed, straight micro-channel was functionalized with antibody that specifically recognized the analytes followed by a downstream analysis region with no CSA packing. We believe the CSA could potentially give us higher collision frequency between analyte and antibody coated particles, with lower fabrication cost and more convenience than building a similar nano-porous structure within the chip. We first detected fluorescein as a model analyte, and then studied type-5 adenovirus capture in buffer and also in cell lysate samples. To our knowledge, this is the first time a CSA based microchip has been reported for immunoassay and immuno-affinity chromatography. Due to the tunable size of the pores and different surface functional groups, this technique is potentially useful for a wide range of analytes important in clinical diagnostics.

The feasibility of a fully packed chip to perform immunoassay was tested using fluorescein and anti-fluorescein with a fully packed bed design. The results from the CCD camera showed good immunoassay performance for a relatively high concentration of fluorescein, with the fluorescence signal distributed across the whole column. Detection can be enhanced by subsequent elution of sample in a concentrated sample plug. To accommodate this approach we added an open segment to the channel as a detection zone.

## 2.2 Experimental

### 2.2.1 Materials

All reagents were prepared in deionized water (Millipore, 18.2 MΩ cm). A dry powder of 2 μm carboxylated silica particles was obtained from Bangs Lab (Indiana, US) and suspended in deionized water with a concentration of 10% (w/v). Sonication was used for around 45 minutes before injection into a microchip. Glass microscope slides were purchased from Fisher and pre-cleaned in hot piranha solution with concentrated sulfuric acid (98%, Caledon Laboratories Ltd.) and hydrogen peroxide (30%, Fisher Scientific) ($H_2SO_4$: $H_2O_2$ = 3:1, v/v) overnight, to make them more hydrophilic. PDMS base and curing agent was obtained from Dow Corning (Sylgard 184, Midland, MI), mixed with a 10:1 (v/v) ratio and cured in the oven overnight. EDC/NHS coupling reagents and pH 4.5 MES buffer and 99.9 % acetonitrile (HPLC grade) were purchased

from Sigma. 50 mM tricine running buffer was prepared in water and adjusted to pH 8.0 with sodium hydroxide. Fluorescein and anti-fluorescein antibody was purchased from Sigma and AbD Serotec (North Carolina, USA) respectively. Crude cell lysate and purified type-5 adenovirus sample were purchased from Vector Biolabs (Philadelphia, USA) and diluted with pH 7.4 PBS buffer. FITC labeled secondary adenovirus antibody was purchased from Fitzgerald Industries International (MA, USA).

2.2.2 Microchip fabrication, colloidal self-assembly and characterization.

Fabrication of a microchip bed by colloidal self-assembly was achieved as previously reported[137]. As illustrated in Figure 2-1, PDMS microchips were fabricated through standard soft lithography by UV patterning a positive photoresist SU-8 master on a 4 inch silicon wafer. PDMS microfluidic channel replicas were then made by casting a mixture of PDMS base and the curing agent with a ratio of 10:1 onto the master, followed by curing under constant heat at 65 °C for around 18 hours. PDMS replicas were peeled off from the master and reservoir holes were then punched to gain access to the channel. Assembly of microchips was accomplished by attaching clean PDMS replicas to clean glass slides. Microchips with a 10 mm straight channel were used, as sketched in Figure 2-2 with a dimension of 100 μm width and 10 μm depths. Mono-dispersed carboxylated silica beads (10% w/v, 2 μm in diameter) were obtained by suspending dried bead powder in deionized water with 30-45

minutes of ultra-sonication before use. A simple 2D mathematical model, shown in Figure 2-1b, was used to calculate the pore size, with r = (1/ (Cos 30°)-1) R= 0.154 R.

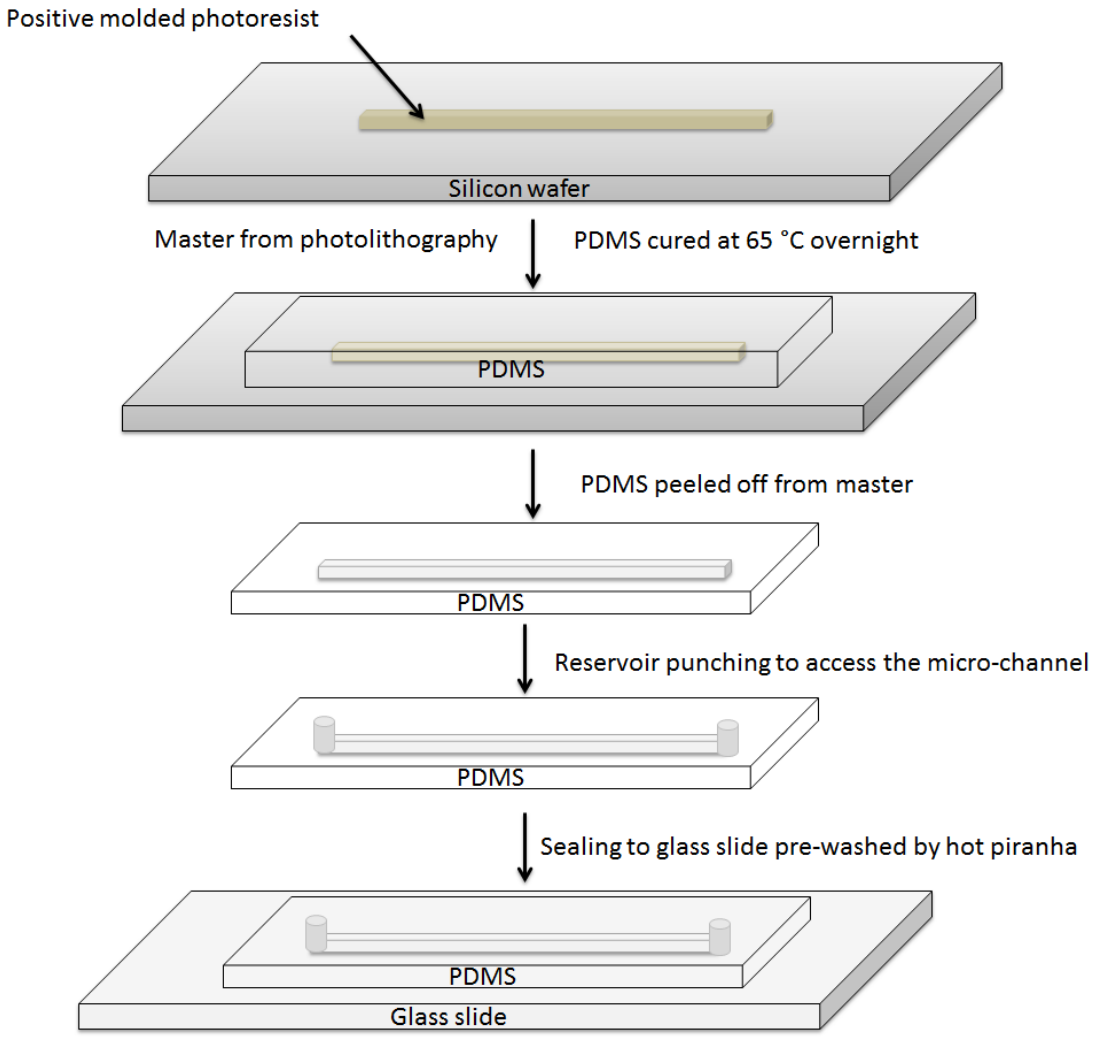


Figure 2-1. Schematic illustration of the soft-lithography process utilized for the fabrication of the device used in this study.

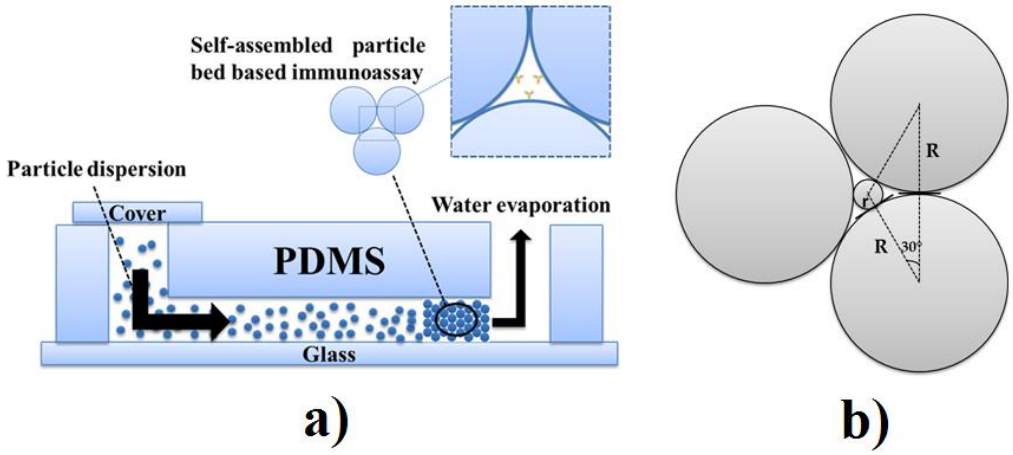


Figure 2-2. a) Structure of capturing antibody functionalized CSA bed based microchip for immunoassay. b) Pore size calculation.

The procedure of microfluidic based colloidal self-assembly is schematically illustrated in Figure 2-2 a). A 10-15 μL colloidal suspension was injected into reservoir 1. The aqueous solution fills the channels spontaneously, forming a liquid meniscus at the outlet of the channel in reservoir 2. Once the channel was filled with the particle suspension, reservoir 1 was covered with a piece of tape or PDMS and reservoir 2 was left open so that evaporation induced crystal lattice self-assembly happens within the channels. A fully packed CSA column is achieved after around 10-15 minutes.

A partially packed chip can be achieved as shown in Figure 2-3. When the crystal length reaches around 1 mm during the crystal lattice growing process, the particle suspension in reservoir 1 was substituted with deionized water,

followed by 3 replicate reservoir washings to avoid further particle injection. The particle suspension left in the channel continued growing until all the particles settled. The length of the particle bed can be controlled to achieve around 6 mm. The overall self-assembly takes around 5-10 minutes.

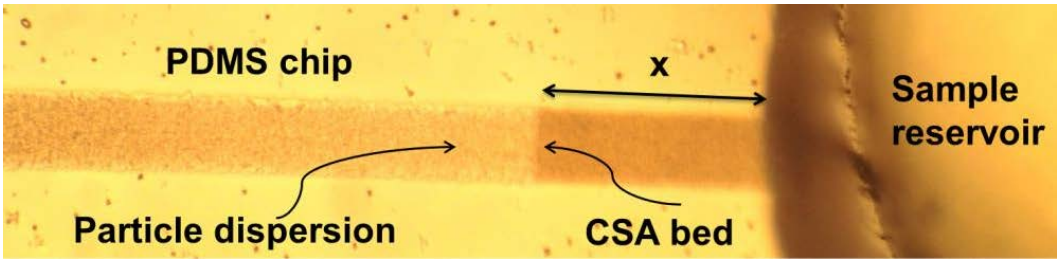


Figure 2-3. Top view of the CSA bed growing inside the micro-channel. The arrows indicate different direction of particle dispersion flow and CSA bed growth. In order to control the length of the CSA bed, the particle dispersion in the injection reservoir was replaced with deionized water when the bed length x reaches around 1 mm using 10% (w/v) particle dispersion and the particles flowing in the channel would continue growing into a 6 mm long bed. The eventual bed length can easily be controlled by maneuvering the timing to replace the particle suspension.

After the colloidal self-assembly within the channel, we then transfer the microchip to a 65 °C oven for 2 hours to induce thermal stabilization process[138]. The dried CSA bed can be recovered by injecting the running buffer into reservoir 1 or other reagents prior to use.

The quality of the colloidal crystals was investigated using scanning electron microscope (SEM, JEOL JSM-6010 LA and LEO 1430) in secondary electron mode. Before taking SEM images, the PDMS molds were peeled off the glass substrate very carefully to avoid structure disturbance. After successful PDMS mold removal, the crystal on the glass substrate was coated with a thin layer of gold (3-4 nm) via a sputtering system (Branson 1200, Triad Scientific, NJ, USA) before SEM analysis. Images were acquired using an electron accelerating voltage of 10-20 kV.

### 2.2.3 Silica carboxyl group activation and antibody conjugation

After baking in the oven, EDC/NHS coupling reagents were used for recovery of the dried bed and to activate the carboxyl group on the silica particles within the microchip, as in Figure 2-4 b). 15 µL of 7 mg/mL NHS and 20 mg/mL EDC in pH 4.5 MES buffer was used for the initial particle surface modification. This process remains at room temperature for 30 minutes. The solution was injected through the sample reservoir by diffusion and manual pressure.

Thumb was used to press the solution through the column. Visual inspection of the column under optical microscope was performed to ensure an intact bed before antibody conjugation. Microchip which was pre-treated with oxygen plasma has been integrated with syringe pump to test the robustness of the

packed bed and the bed showed good stability under 0.5-1.0 μL/min flow rate for 30 minutes. However, replacing the sample in the reservoir will trap air bubble in the column, which is difficult to remove under the applied flow rate. Confirmed EOF is a superior driven force in this case due to its capability to provide continuous flow for sample delivery without damaging the bed.

After the solution reached the end of the dried CSA bed, reservoir 2 was then covered to prevent the solution going further. After 30 minutes, the reservoir was emptied and injected with the first, capture antibody. The solution flowed by manual pressure to replace the free EDC/NHS within the structure, and was immobilized on the surface of the silica particle through amine functionality on the protein and the activated carboxyl group. This antibody conjugation proceeded for 30 minutes at room temperature. For the partially packed chip, the difference between an empty channel and a channel filled with solution is revealed by the reflection of the channel under light, providing an indication of the fluid flow as a check on the pressure driven flow method utilized. In our experiments, either $5 \times 10^{-3}$ mg/mL of anti-fluorescein antibody or $2 \times 10^{-2}$ mg/mL anti-adenovirus antibody was injected in reservoir 1 for 30 minutes to build the capturing bed as illustrated in Figure 2-4.

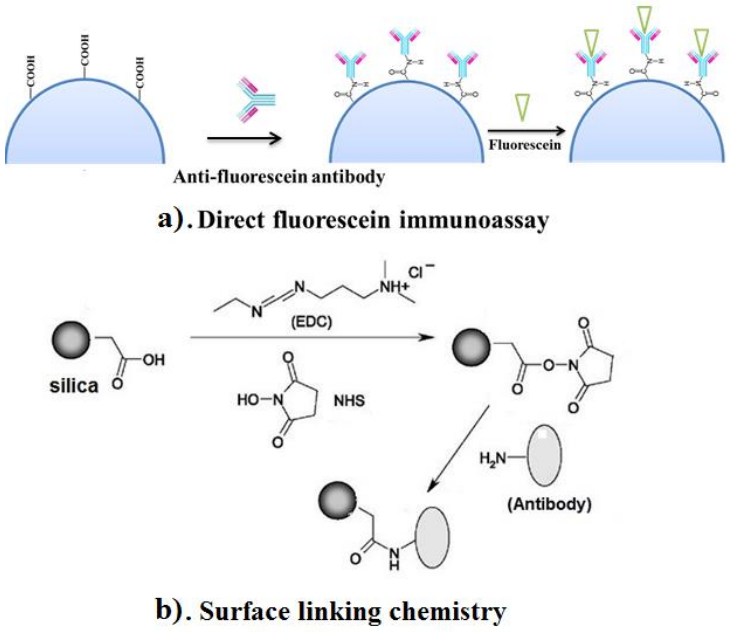


Figure 2-4. Schematic illustration of direct immunoassay using fluorescein and anti-fluorescein. a) is process of the immunoassay. b) Covalent linking of first capturing antibody to the particle bed.

### 2.2.4 Instrumental setup

The confocal epifluorescence microscope setup is shown in Figure 2-5. Fluorescent samples were excited with an expanded 488-nm argon ion laser beam, and the emission was collected with a StallaCam astronomy CCD camera and a high-sensitivity PMT, an inverted microscope equipped with a 505 DRLP dichroic mirror, 515-nm long pass filter, and a 25/0.35 NPL Fluotar objective (Leitz Wetzlar). Fluorescence signal was transmitted to a Labview Program

(National Instruments) developed by our group and data was analyzed by Origin 9.0.

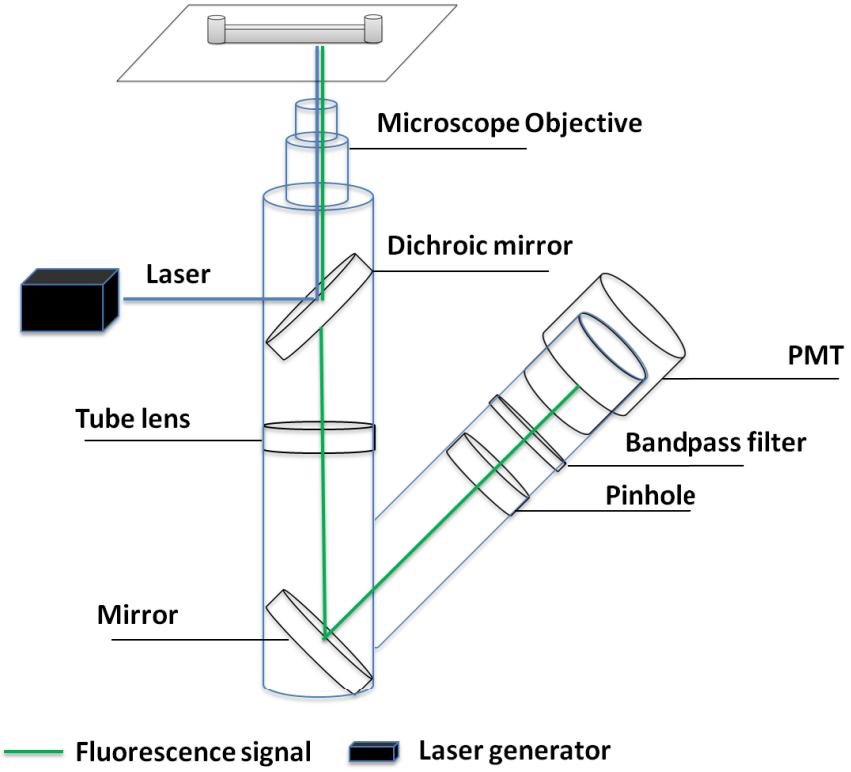


Figure 2-5. The setup of the epifluorescece microscopy.

2.2.5 Direct immunoassay for fluorescein

Fluorescein and anti-fluorescein antibody were used as a model antibody-antigen immunoassay, as shown in Figure 2-4 a. A fully packed column was used and activated with EDC/NHS (Figure 2-4 b) to test the efficiency of antibody conjugation and the ability to perform immunoassay. After the CSA bed was modified with EDC/NHS, 20 μL of $0.5 \times 10^{-3}$ mg/mL anti-fluorescein antibody

was injected to reservoir 1, flowed through the activated carboxyl silica packed column, then allowed to sit stationary for 30 minutes at room temperature. Slight manual pressure was applied to facilitate the solution flow. The chip was then mounted under the epifluorescence microscope after a 30 minute conjugation. Electrodes were inserted into each of the two reservoirs to apply electric field. 80 V was applied to this 1.0 cm long channel in each of the following washing and sample loading step. 50 mM pH 8.0 tricine buffer was used as the running and washing buffer. After the system setup, the sample reservoir which contains the first antibody was replaced by 50 mM pH 8.0 tricine running buffer to wash the unbound antibody by EOF and to quench the unreacted EDC/NHS. After 15 minutes of running, $1.4 \times 10^{-4}$ mg/mL fluorescein dissolved in DMSO and premixed with running buffer sample was injected to reservoir 1 for 30 minutes for incubation, followed by 15 minutes of washing with running buffer. The fluorescence signal emitted by the captured fluorescein was captured by a CCD camera, which collects the fluorescence image at 10 fps. A control experiment was performed under the same conditions, but lacking the step of primary antibody conjugation. The same antibody conjugate was applied to a partially packed column (0.6 cm out of 1.0 cm), with an additional releasing step to the particle free empty downstream analysis area. A PMT was used as the detector. The releasing step was performed after 15 minutes of washing with running buffer until the signal dropped to the baseline. 20 μL of 99.9 % acetonitrile was used as the eluent to release the captured fluorescein. The plug of fluorescein

released from the bed moved through the micro-channel, was excited by the 488 nm argon laser, and detected by PMT, transmitted to the Labview program and analyzed by Origin 9.0.

2.2.6 Sandwich immunoassay for inactivated type-5 adenovirus in partially packed chip for immuno-affinity chromatography.

Type-5 adenovirus with a size of 80-100 nm was employed as a target analyte, as a demonstration of a sandwich immunoassay in the partially packed chip. The process is described as in Figure 2-12 (B). A partially packed chip was modified by EDC/NHS for 30 min after thermal stabilization, followed by adenovirus capture antibody conjugation for 30 min. Diffusion and manual pressure were the major driving force for the EDC/NHS and first antibody motion in the chip. After the first antibody conjugation, the chip was mounted to the epifluorecence microscope. The same tricine buffer was used as the running and washing buffer. 80 V was applied to this 1.0 cm long channel for all later samples loading and washing. After the system setup, pH 8.0 tricine buffer was used to replace the first antibody in the sample reservoir, to wash the chip of unbound antibody for 15 min under 80 V/cm and to further quench the EDC/NHS coupling reaction to proteins. In order to prevent non-specific absorption of antibody or virus to the silica particle surface, BSA 1% (w/v) was used as the blocking reagent. BSA was loaded for 15 minutes at 80 V/cm followed by a 15 minute washing step. Different concentrations of type-5 adenovirus sample were loaded for 30 min

under the same conditions, followed by a buffer washing for 15 min. A FITC labelled secondary antibody that recognizes the Hexon protein on the virus surface was then loaded for 30 min. Buffer washing for around 15 min to remove the excess unbound FITC labeled secondary antibody was performed until the fluorescence signal dropped to the baseline. To release the captured secondary antibody or virus/secondary antibody complex, 20 μL of pure acetonitrile was used as the eluent. Control experiments were done in which either the first capture antibody was not loaded, or a blank cell lysate sample without viruses was used. Cell lysate samples were used as real sample tests.

## 2.3 Results and Discussion

### 2.3.1 Colloidal self-assembly and thermal stabilization

The growth of CSA beds was achieved following previously reported methods[60,64,65,137], as schematically illustrated in Figure 2-3. CSA crystal formation begins after the particles arrive at the sample reservoir. The arrows in Figure 2-3 indicate the moving direction of the particle dispersion and the direction of growth of the bed. For a fully packed column, it usually takes around 10-15 minutes to finish the packing. For a partially packed chip, empirically, once the length of the CSA bed reaches 0.1 cm, by replacing the particle dispersion in the waste reservoir with water and covering it back with a piece of PDMS or tape, the leftover particles in the channel continue to

crystallize to give an approximately 0.5-0.6 cm long bed. The length of the bed can be maneuvered easily by choosing the time for particle suspension substitution. A shorter bed such as 0.2-0.3 cm, gives the risk of virus particles escaping the bed. However, a 0.7-0.8 cm long bed, gives a higher back pressure[126]. So we choose a particle bed with a length of 0.6 cm out of 1.0 cm.

The finished chip was tested with an electric field applied between the two terminals of 30 V/cm. Our first test used fluorescein. We observed obvious destruction of the bed, as shown in Figure 2-6 a and b. The images were taken using an optical microscope before and after applying the external electric field. By comparing the packing density in the column, we can clearly see the destruction of the bed after applying voltage. Figure 2-6 c shows a frame grab of a video taken with the epifluorescence microscope. The video clearly shows particle flow with applied voltage. The reason for the particle flow may be the surface charge of the surface carboxyl groups, creating electro-osmotic forces on the particles in the running buffer. Clearly, we need a stable capture bed that can withstand voltage in order to deliver the analytes.

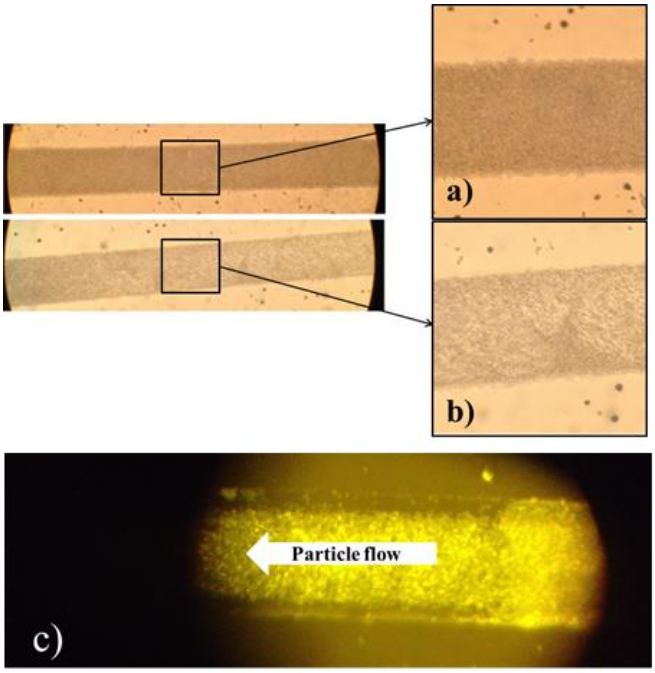


Figure 2-6. Pre-thermal stabilization results. a) and b) are the zoomed out results from a fresh packed chip before and after applying external electric field under 30V/cm for 15 minutes. c) is an image taken from the epifluorescence microscope which indicates the particle flows with the EOF.

To increase the bed stability we chose a thermal stabilization technique reported by Ceriotti, L. et al.[138] due to its efficiency and simplicity for this specific application. Adapting this technique, we baked our chip in an oven at 65 °C constant temperature for 2 hours. The efficiency of the thermal treatment was again evaluated with an electric field, driving fluorescein through the channel. We repeated the stability tests on a fully packed column 4 times with each trace shown in Figure 2-7. The bed was inspected visually between runs to confirm they remained intact. Also, the breakthrough time would have changed if the bed

was destroyed due to the shift of EOF. Figure 2-7 a shows the breakthrough of fluorescein, while b shows the washing step. We also studied the fluorescence breakthrough time with different voltage ranges from 30 V/cm to 80 V/cm, as shown in the inserted graph in Figure 2-7 b. Thermal stabilization time and temperature were also evaluated for the chip stability as shown in Table 2-1. The final choice for thermally stabilizing the fully packed column was 2 hours at 65 °C. Cracks were still induced by applying 100 V/cm for about 15 minutes, so we chose 80 V/cm as our running voltage.

Several possible mechanisms were mentioned in reference. Silica particle sintering requires temperature of above 260 °C.[138] Interparticle bonding also was proposed to provide as the mechanism in a microparticulate silica columns stabilization study, with a temperature involved up to 300 °C to 400 °C.[139] Consequently silica sintering and interparticle bonding are not likely to explain the increased stability we see based on the temperature we applied. The authors also suggest some shrinkage of the PDMS during heating, and increased particle-wall interactions associated with a small change in size of the capillary channel upon heating the silicone. Given the low temperature we used, these latter two explanations are most likely.

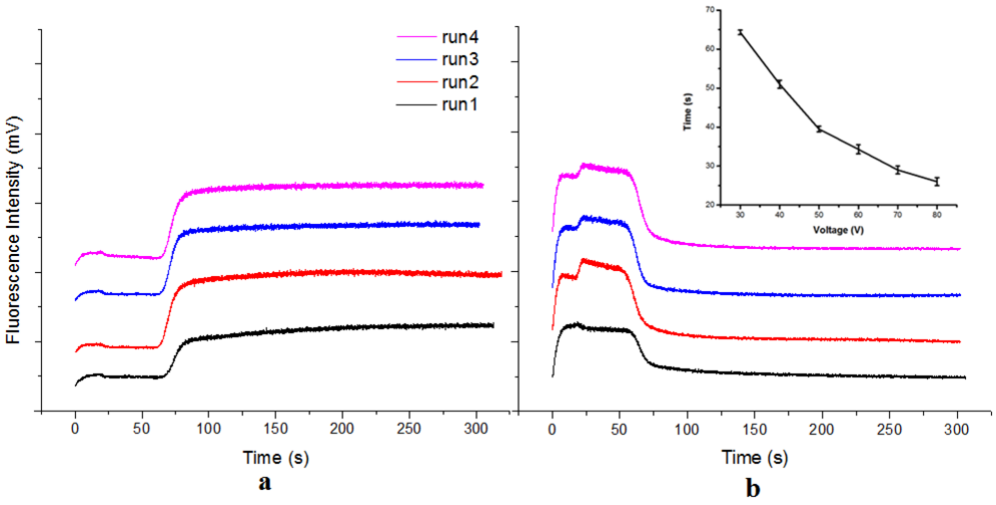


Figure 2-7. The fluorescein loading results in a fully packed chip after thermal stabilization. Inserted is the study between the voltage (30-80 V/cm) and the breakthrough time. Distance of the sample reservoir and the laser point was set up as 0.6 cm.

Table 2-1. Thermal stabilization time and temperature study.

| Baking Temperature (°C) | Baking time (h) | Performance |
|---|---|---|
| a 65 | 3 | √ |
| a 65 | 2 | √ |
| a 85 | 1.5 | × |
| a 85 | 1 | × |
| a 85 | 0.5 | × |
| a 100 | 1 | × |
| a 120 | 0.5 | × |
| b 65 | 2 | √ |
| b 85 | 0.5 | × |

* a represents fully packed chip while b represents partially packed chip.

We applied the same thermal stabilization method for partially packed chips. Optical images were taken before and after the thermal stabilization shown in Figure 2-8. The packed column turned to black due to the drying, which arises from the change in reflective index of the dry bed. The particle interface change seen in Figure 2-8 a and b may also indicate some rearrangement of the packing, due to the physical compression from the shrinkage of the PDMS. SEM images were taken before and after the thermal stabilization and no obvious damage to the bed was observed using 65 °C for 2 hours.

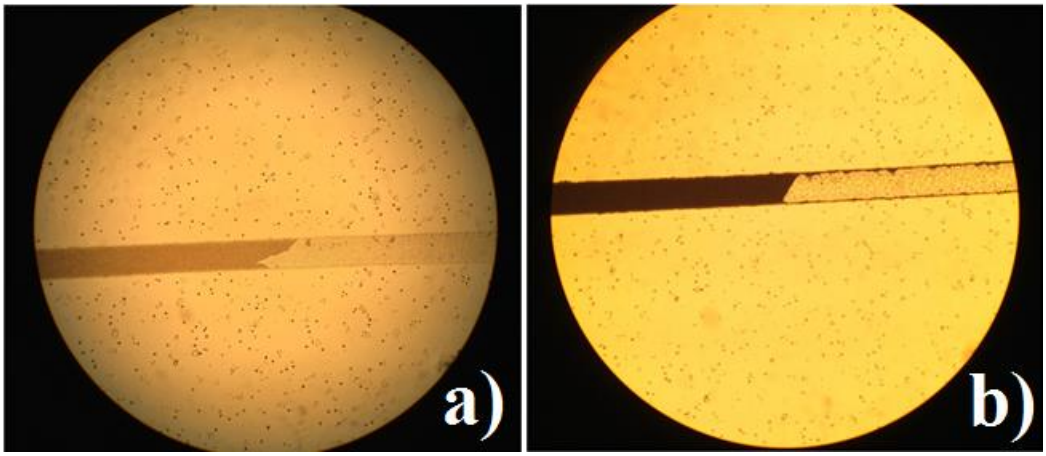


Figure 2-8. Partially packed chip thermal stabilization results. a) and b) are before and after thermal stabilization images taken by optical microscope.

We repeated the fluorescein loading process on a thermally stabilized, partially packed chip 5 times at a voltage of 80 V/cm; the results are shown in Figure 2-9. Figure 2-9 c shows the loading of fluorescein sample through the column while Figure 2-9 d shows rinsing using running buffer. SEM images were taken to see the quality of the CSA bed and the results are shown in Figure 2-9 b. After

peeling off the PDMS from the glass slides, a layer of gold was sputtered onto the surface. The surface layer was partially disrupted while removing PDMS from the glass slide, but the magnified image shows good packing quality and high order in unaffected regions.

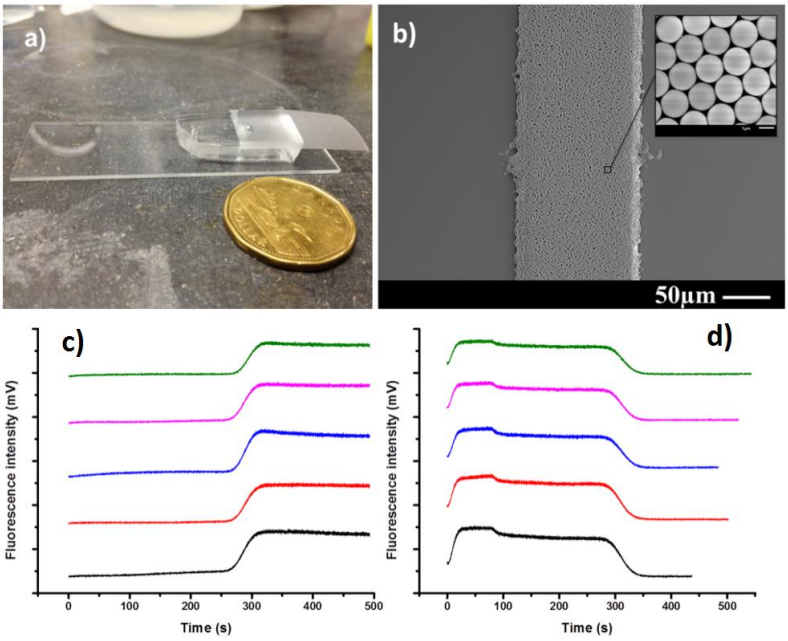


Figure 2-9. Illustration of colloidal self-assembly within microchip and characterization. a) Microchip integrated with CSA bed. b) SEM images of the CSA bed on the glass slide after peeling off the PDMS and sputtered the surface with gold. A partially packed chip stability tests using fluorescein for signal detection after thermal stabilization. c) Repetitive results of fluorescein flowing through the thermally treated microchip. d) Buffer washing of the fluorescein in the channel.

### 2.3.2 Evaluation of modified bead-based microchip for immunoassay using a fully packed column.

We utilized fluorescein and anti-fluorescein antibody as the model analyte to test the efficiency of the microchip for immunoassay. Activation of carboxyl silica particles and immobilization of anti-fluorescein capture antibody was accomplished by slight manual pressure. All the following sample loading and washing steps were performed under electric field after mounting the chip to the epifluorescence microscope. A 50 mM pH 8.0 tricine buffer was utilized as the running and washing buffer. 80 V were applied to the 1.0 cm long channel for all the sample loading and washing steps. After 30 minutes of primary antibody conjugation, the sample reservoir was refilled with 50 mM pH 8.0 tricine buffer, to allow rinsing for a further 15 minutes. A sample of fluorescein pre-mixed with pH 8.0 tricine running buffer was injected and incubated for 30 minutes. Then buffer was applied to wash the free fluorescein from the channel until the signal dropped to the baseline. A CCD camera was used to collect the image signal from the channel, as illustrated in Figure 2-10. Figure 2-10 A, C, E are three different chips loading fluorescein results. While B, D, and E are the corresponding results after 15 minutes of buffer washing. Figure 2-10 A shows a chip that was packed with pre-functionalized beads, which could not be used for thermal stabilization. Figure 2-10 B shows cracking still happens inside the channel after running the sample. Figure 2-10 C shows a chip that was thermally stabilized and functionalized with capturing antibody on-chip, which shows

good immunoassay performance. Figure 2-10 E shows a thermal stabilized blank control chip without any capturing antibody conjugation, which gives no signal after buffer washing in Figure 2-10 F.

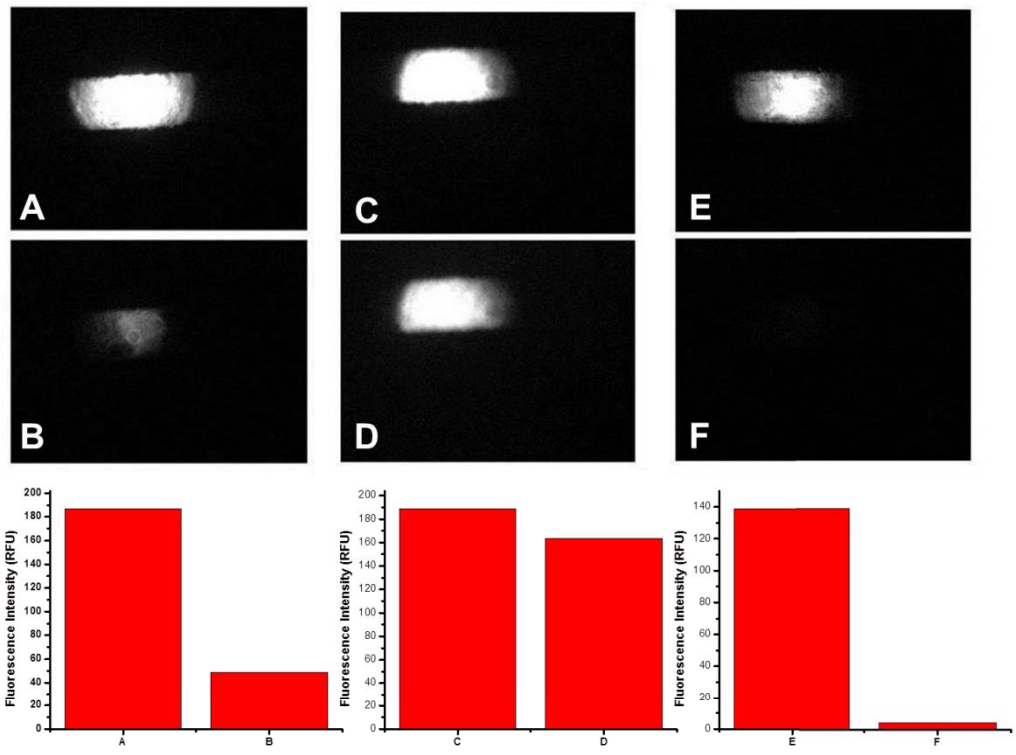


Figure 2-10. Direct immunoassay using fully packed column. A), C), E) are fluorescein loading process while B), D) and F) are after free sample washing. Image was taken by CCD camera. Different chips were used in this series of experiments. Chip A) was packed with pre-functionalized using anti fluorescein antibody; C) was functionalized after the packing and thermal stabilization. E) was a blank control experiment without any antibody functionalization.

### 2.3.3 Immuno-affinity chromatography for fluorescein using a partially packed column.

The fluorescence signal scattering in the fully packed column posts challenge for detection, especially for really low concentration virus capture. Eluting to release and concentrate the captured signal molecules would be able to provide a better sensitivity. The basic principle of immuno-affinity chromatography was illustrated in Figure 2-11. Instead of detecting the whole column, a elution step is required to release the captured analytes, which will be collected for further analysis.

The same fluorescein immunoassay was performed for immuno-affinity chromatography. However, instead of using a CCD camera to capture the fluorescence images of the bed, we used acetonitrile as an eluent to allow detection downstream. Sample was driven through the channel by the same voltage to release the captured fluorescein, for detection at the downstream PMT. The immuno-affinity chromatography procedure is outlined in Figure 2-12. Figure 2-13 a) shows the elution peak of 4.51 nM fluorescein captured by the functionalized packed column. Blank control experiments were performed without fluorescein sample in buffer Figure 2-13 b) or without the first capturing antibody Figure 2-13 c), which showed no significant response. The column was regenerated by reconditioning the column with running buffer, at 30 V/cm for 30 minutes. The same immuno-affinity capture was performed 5 times. The elution

peak area dropped by 75 % at the fifth run as shown in Figure 2-14. The decline is consistent with denaturing of the antibody during the acetonitrile elution step.

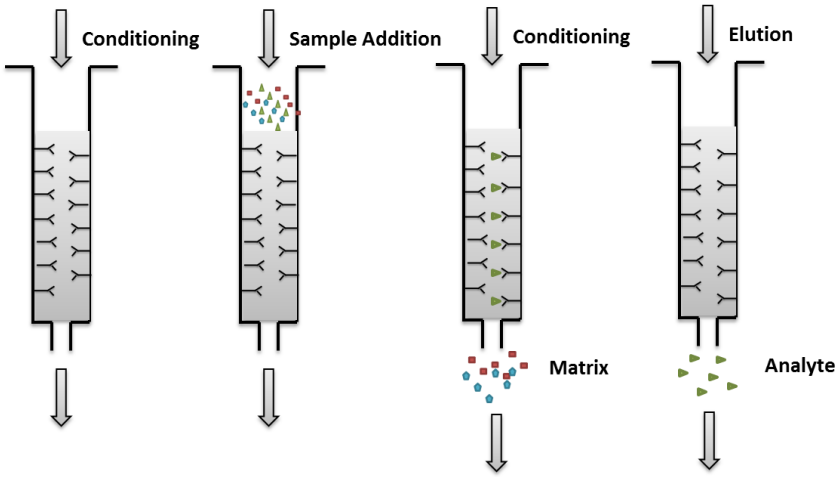


Figure 2-11. Principle of immuno-affinity chromatography.

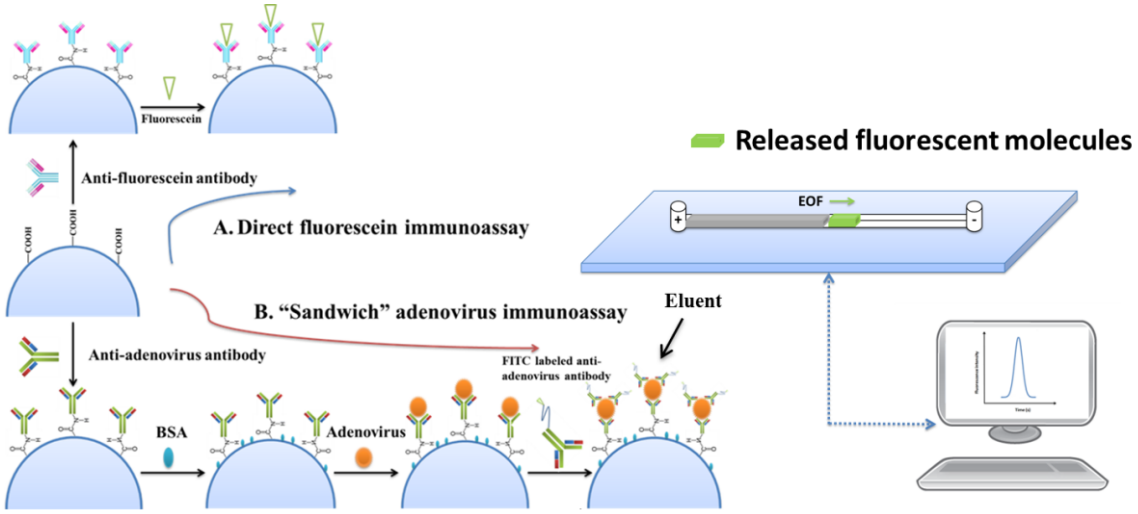


Figure 2-12. Schematic of beads based direct fluorescein immunoassay (A) and "Sandwich" immunoassay for inactivated type-5 adenovirus (B). After capturing, an eluent was applied to release the analyte plug with fluorescence from the captured bed and being detected by the instrument.

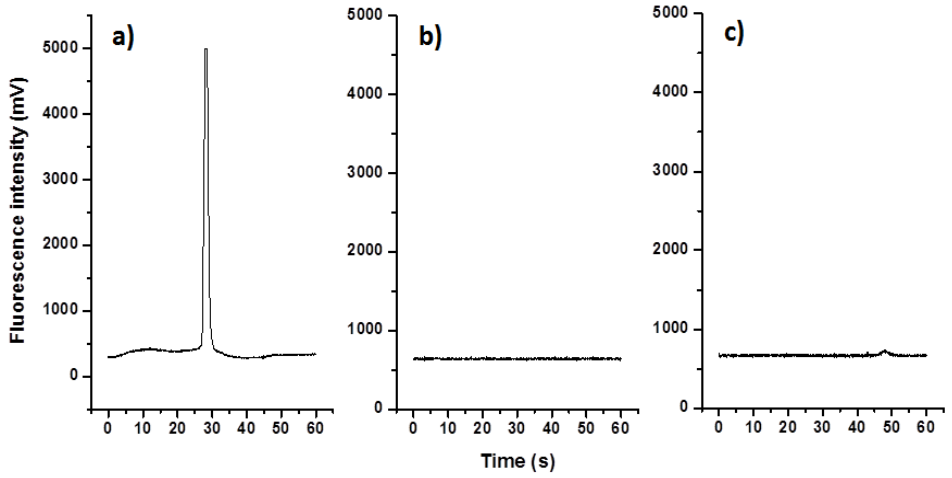


Figure 2-13. Determination of the efficiency of the immunoassay using functionalized CSA. a). Elution profile of 4.51 nM of fluorescein. b). Blank fluorescein free sample flowing through the functionalized CSA microchip. c). CSA bed without primary capture antibody conjugation;

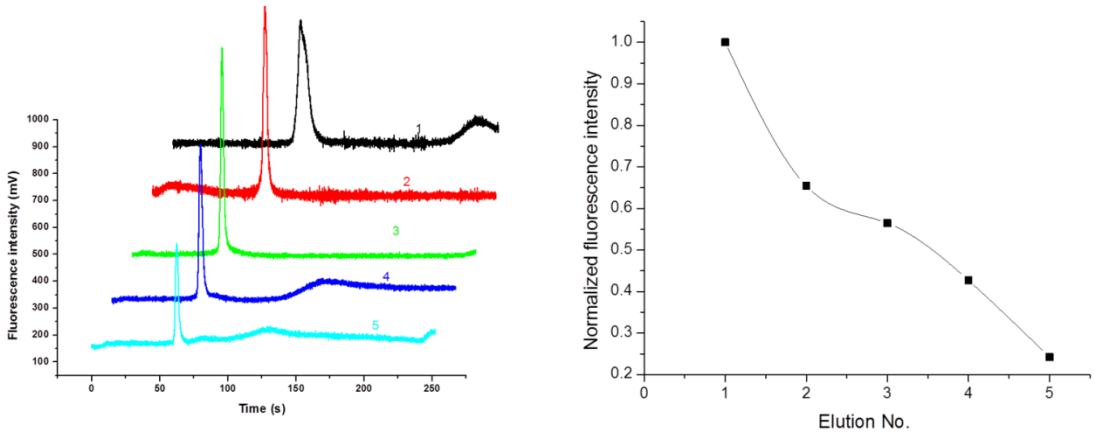


Figure 2-14. Column regeneration results by re-conditioning with running buffer. Peak area dropped 75% after fifth run.

### 2.3.4 Immuno-affinity chromatography for deactivated type-5 adenovirus

A "sandwich" immuno-affinity chromatography of deactivated type-5 adenovirus was demonstrated here. After thermal stabilization and carboxyl group activation by EDC/NHS, the packed column was loaded with anti-type 5 adenovirus antibody as the primary immobilized antibody. Flow was driven by slight manual pressure. The chip was then transferred and mounted on the fluorescence microscope, with electrodes inserted in the sample and waste reservoirs. A 50 mM pH 8.0 tricine buffer was used as the running and washing buffer. 80 V was applied to this 1.0 cm long channel in the following sample loading and washing steps. After washing the excess unbound primary antibody from the column, 1 % (w/v) BSA was applied to prevent non-specific adsorption of virus or secondary antibody on the column for 15 minutes, followed with a 15 minute wash. A 20 μL aliquot of different concentrations (0, $5.0 \times 10^3$, $1.0 \times 10^4$, $2.5 \times 10^4$, $5.0\times 10^4$, $1.0 \times 10^5$ VP/mL) of adenovirus in PBS buffer was delivered into the column. A new column was used for each concentration. The virus sample loading step was kept constant at 30 minutes. After 15 minutes of washing, a secondary antibody, labeled with FITC, was loaded for 30 minutes to interact with primary antibody-virus complex on the surface of the column. A 20 μL aliquot of 99.9 % acetonitrile was used as the eluent after first washing the free unbound secondary antibody in the column. Fluorescence signal was collected when the plug of the secondary antibody passed through the laser spot

downstream. Elution takes around 60 seconds. A second elution was used to make sure the elution was complete.

The experimental procedures and a typical data set including all the steps involved in this assay of virus particles are shown in Figure 2-15. A calibration curve (Figure 2-16) was established based on the peak area observed, with a dynamic range of $5.0 \times 10^3$ to $1.0 \times 10^5$ VP/mL. Each data point was collected from a freshly made chip. The least squares fit weighted by the standard deviation in the three replicate data, gave a slope of $0.053 \pm 0.0043$ and intercept of $469.14 \pm 75.90$, $r=0.986$, $R^2=0.967$. The relative standard deviation in predicted concentration would be 16.25 % for an observed signal in the mid-range ($y=2000$). The limit of detection was calculated as $8.3 \times 10^3$ VP/mL (3 SD/k, SD is the standard deviation of the blank whereas the k is the slope of the calibration curve) for a 20 μL sample volume. The detection limit is 20 times lower than previously reported using a polymer membrane as the pre-concentration method[132], which is a significant improvement towards the goal of clinical diagnosis.

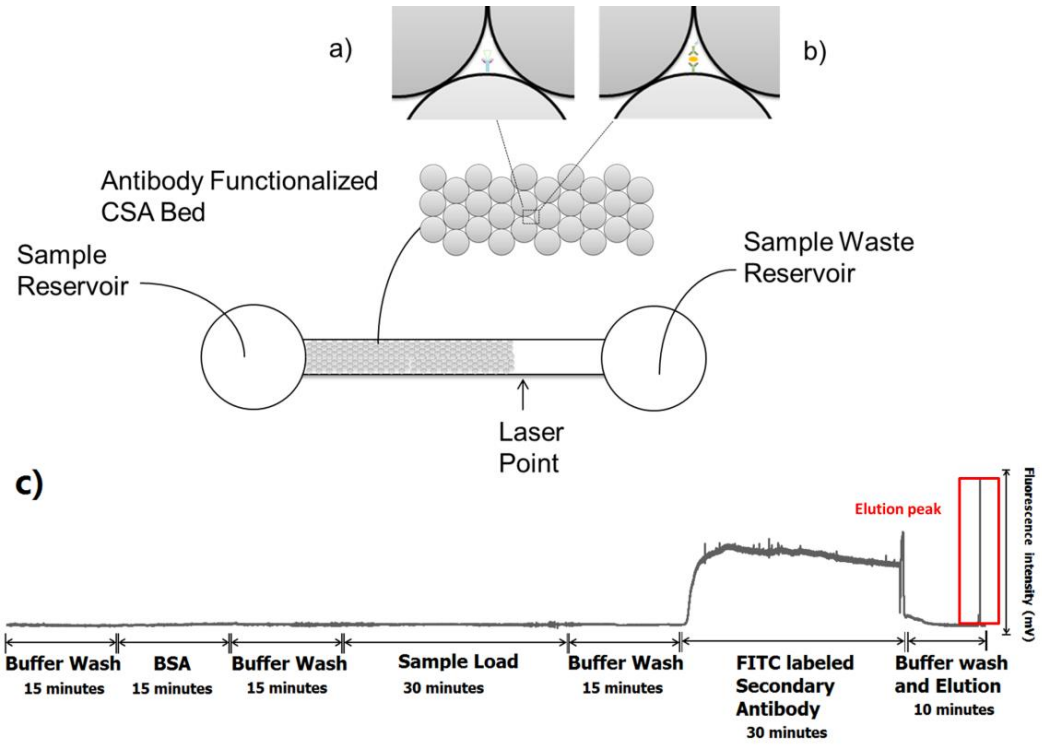


Figure 2-15. Immunoassay set-up in the CSA based microchip and signal response. Fluorescein a) and type-5 adenovirus b) capturing using beads based microchip. Schematic illustration of the microchip used for capturing and releasing with the antibody functionalized CSA in the channel. The laser point is located in downstream particle-free zone for eluting plug analysis.

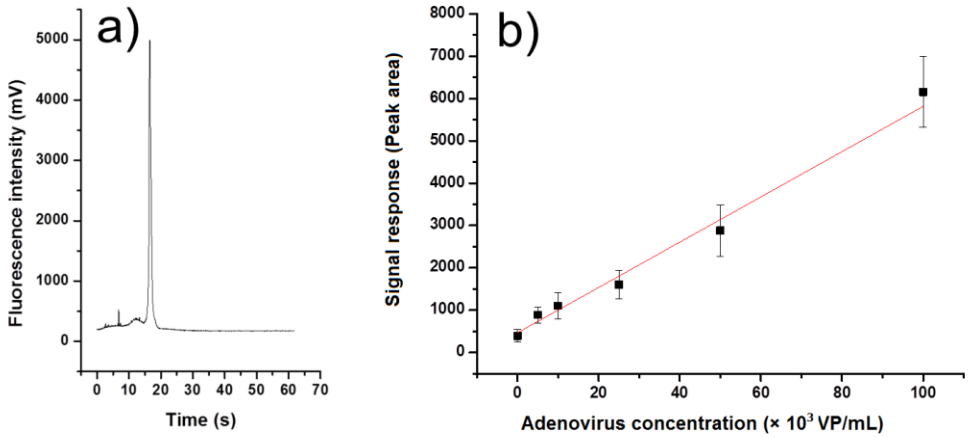


Figure 2-16. a) Elution peak for $5.0 \times 10^4$ VP/mL type-5 adenovirus in PBS buffer. b) Response curve with different concentration of adenovirus.

Adenovirus in crude cell lysate sample ($1.5 \times 10^3$, $2.5 \times 10^3$, $3.5 \times 10^3$, $5.0 \times 10^3$ PFU/mL) was also detected in this device and the lowest concentration that could be detected was $1.5 \times 10^3$ PFU/mL (Figure 2-17). Control experiments results without either virus in cell lysate sample or without first capturing antibody were shown in Figure 2-18. No obvious peak signal was observed. The viral particle (VP) number of the pure virus sample is $5.0 \times 10^{12}$ VP/mL according to the manufacturer, which includes the live and dead virus particles. The VP number was measured by optical density at 260 nm for the viral DNA and proteins as we received. The plaque forming unit (PFU) count for this sample was $1.4 \times 10^{11}$ PFU/mL, indicating most of virus was dead. The dead virus particles arising during sample preparation vary significantly, and according to the manufacturer, the ratio between dead viruses to active ones

usually falls in a range of 20 to 50. The viral particle numbers in the crude cell lysate virus sample was not measurable, due to the presence of other proteins and probable particles. The plaque forming unit was determined to be $1.0 \times 10^{10}$ PFU/mL by the manufacturer. An amplification process after receiving the sample was utilized, performed by infecting the human HEK 293 cells in a tissue culture dish. The PFU number for this amplified product, determined by counting the number of infected cells, was $1.0 \times 10^{11}$ PFU/mL. Aliquots with different concentrations of viral particles were diluted from the sample following 30 minutes of thermal inactivation (70 °C) to kill the virus. We assume the ratio of dead to live in this incubated cell lysate again follows a 20 to 50 range. For the crude cell lysate sample, the lowest number of viral particles detected was estimated as $3.0 \times 10^4$ VP/mL to $7.5 \times 10^4$ VP/mL.

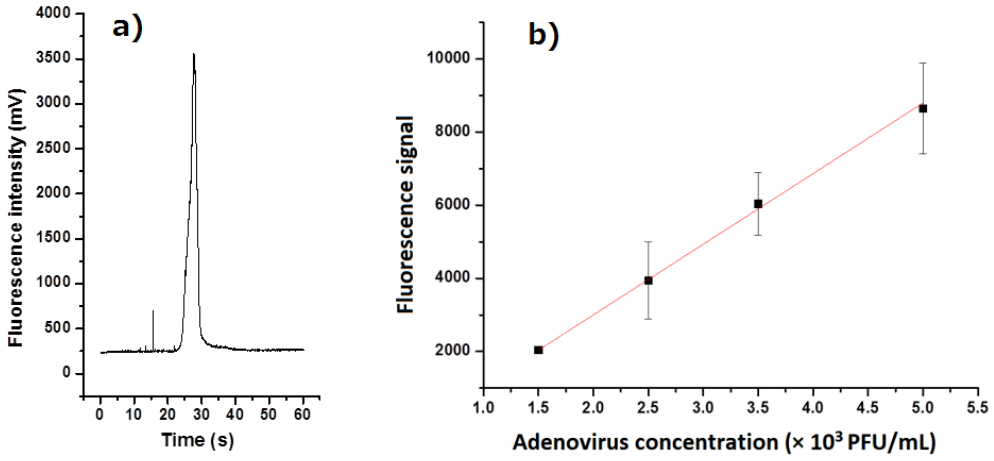


Figure 2-17. a) Elution profile of $5.0 \times 10^3$ PFU/mL type-5 adenovirus in cell lysate sample. b) Calibration curve of type-5 adenovirus in cell lysate sample. Lowest concentration for this device is $1.5 \times 10^3$ PFU/mL.

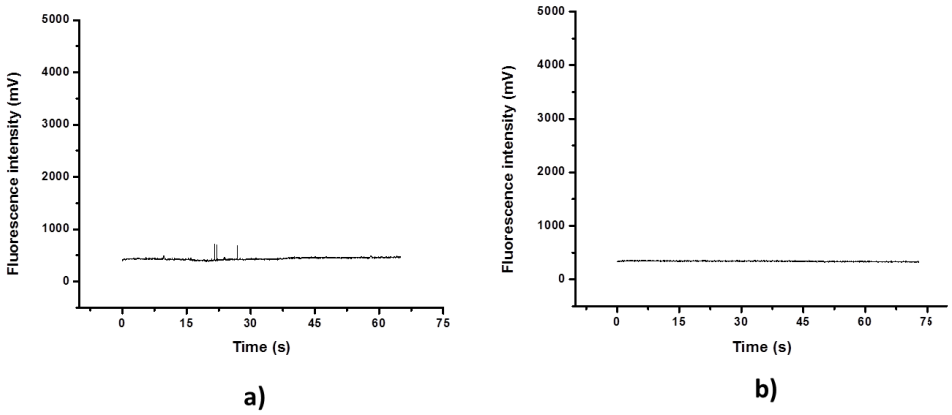


Figure 2-18. Control experiments on adenovirus in crude cell lysate sample. a) is the blank cell lysate sample while b) is the result without any primary antibody conjugation.

## 2.4 Conclusion

We fabricated a bead based microfluidic chip to perform immunoassay and immuno-affinity chromatography for virus capture. A tortuous path bed with around 300 nm pores was prepared by colloidal self-assembly of 2 μm silica particles with carboxyl groups on the surface. A fully packed column was used and proved the feasibility of the chip based immunoassay. Then the particles were self-assembled within a micro-channel 10 μm × 100 μm in size, forming a 0.5-0.6 cm long bed, leaving a 0.4-0.5 cm empty bed downstream the analysis region. By modifying with EDC/NHS, we immobilized anti-fluorescein antibody or type-5 adenovirus antibody. The tortuous path of the hexagonal close packed crystalline particle array ensures that frequent collisions of the virus with the particles that define the walls of the nano-porous structure will occur, offering a highly effective fluidic design for virus capture. The devices can capture fluorescein as a demonstration and positive control study, and viruses for an assay. A 4.81 nM fluorescein solution concentrated using anti-fluorescein antibody and released with an eluent gave a huge signal. Similar experiments were performed for the type-5 adenovirus. The limit of detection was calculated as $8.3 \times 10^3$ VP/mL for 20 μL pure adenovirus sample, and the lowest concentration can be detected in crude cell lysate sample was $1.5 \times 10^3$ PFU/mL (20 μL). Due to the easy and cost effective fabrication process, and the tunable particle surface and size, this technology has great potential applications for micro-organisms and other analytes detection.

## 2.5 Acknowledgements

The authors thank University of Alberta for support in Nanofab and also Department of Chemistry for the support from Biological Services.

# Chapter 3 Conclusions and future work

### 3.1 Summary of this thesis

Objective of this thesis is to fabricate a colloidal self-assembly based microchip and to explore its application in immunosorbent assay for pathogen detection. A functionalized bead based microchip that can perform immunoassay and immuno-affinity chromatography for virus capture was successfully fabricated. 2 μm carboxylated silica particles were used for colloidal self-assembly within microchannel to form a porous tortuous path bed. The micro-channel used for the particle self-assembly was 10000 μm × 100 μm × 10 μm in size. We first demonstrated immunoassay using fluorescein and anti-fluorescein antibody with a fully packed CSA column. Then a partially packed chip was achieved and successfully been used for immuno-affinity chromatography. The packed bed length is about 0.5-0.6 cm, leaving a 0.4-0.5 cm empty bed downstream analysis region. Anti-fluorescein or anti-adenovirus was immobilized onto the particle surface, followed by sample loading. The captured target molecules were then eluted by using acetonitrile after antibody-antigen incubation.

The tortuous path of the hexagonal close packed crystalline particle array ensures that frequent collisions of the virus with the particles that define the walls of the nano-porous structure will occur, offering a highly effective fluidic design for virus capture. The results showed that the devices can capture

fluorescein as a demonstration and positive control study, and viruses for an assay. Using anti-fluorescein antibody and released with an eluent, a 4.81 nM fluorescein solution was concentrated to give a huge signal. Similar experiments were performed for the type-5 adenovirus in pure buffer sample and in cell lysate sample. The limit of detection for the pure adenovirus sample was calculated as $8.3 \times 10^3$ VP/mL, with a dynamic range of $5.0 \times 10^3$ to $1.0 \times 10^5$ VP/mL. The lowest concentration can be detected in cell lysate sample was $1.5 \times 10^3$ PFU/mL.

Due to the easy and cost effective fabrication process, and the tunable particle surface and size, this technology has great potential applications for micro-organisms and other analytes detection.

**3.2 Future work**

The present design using colloidal self-assembly in a single straight channel as the capture matrix showed successful immunoassay with type-5 adenovirus. In order to further increase the binding capacity and sensitivity, it might possible to redesign the microchip into a multichannel structure, which serves as an amplification mechanism.

Another critical measurement capability is detection of multiple analytes while conducting just one single assay.[140] Multiplexing has the potential leading to a

faster detection[141], higher throughput[142] and reduced sample consumption.[143,144] For beads based multiplexing assays, modification of beads with various analytes is the core strategy. Combined with the successful colloidal self-assembly based protein separation[60], the redesigned multichannel microchip can first packed with particles to form a porous tortuous structure, and a mixture of different kinds of antibodies can be applied to form a specific capturing matrix. Instead of using an empty channel as the downstream analysis region, a channel packed with smaller particle can be used for different secondary antibodies separation. Multiplexing detection can then be achieved by identifying each individual separation peak.

To summarize, this thesis reports experimental study of the fabrication of a bead based microchip for immunoassay and immuno-affinity chromatography. Due to the simple fabrication and low cost, this technology has the potential to be commercialized for mass production of disposable diagnostic tool.

## References


(1) Manz, A.; Graber, N.; Widmer, H. á. *Sensors and actuators B: Chemical* **1990**, *1*, 244-248.

(2) Reyes, D. R.; Iossifidis, D.; Auroux, P.-A.; Manz, A. *Analytical chemistry* **2002**, *74*, 2623-2636.

(3) Manz, A.; Harrison, D. J.; Verpoorte, E. M.; Fettinger, J. C.; Paulus, A.; Lüdi, H.; Widmer, H. M. *Journal of Chromatography A* **1992**, *593*, 253-258.

(4) Whitesides, G. M. *Nature* **2006**, *442*, 368-373.

(5) Duffy, D. C.; McDonald, J. C.; Schueller, O. J.; Whitesides, G. M. *Analytical chemistry* **1998**, *70*, 4974-4984.

(6) Sackmann, E. K.; Fulton, A. L.; Beebe, D. J. *Nature* **2014**, *507*, 181-189.

(7) Beebe, D. J.; Mensing, G. A.; Walker, G. M. *Annual review of biomedical engineering* **2002**, *4*, 261-286.

(8) Hagen, T. *Biochem Anal Biochem* **2012**, *1*, e108.

(9) Foudeh, A. M.; Didar, T. F.; Veres, T.; Tabrizian, M. *Lab on a Chip* **2012**, *12*, 3249-3266.

(10) Han, K. N.; Li, C. A.; Seong, G. H. *Annu Rev Anal Chem* **2013**, *6*, 119-141.

(11) Yager, P.; Edwards, T.; Fu, E.; Helton, K.; Nelson, K.; Tam, M. R.; Weigl, B. H. *Nature* **2006**, *442*, 412-418.

(12) Morens, D. M.; Folkers, G. K.; Fauci, A. S. *Nature* **2004**, *430*, 242-249.

(13) Fauci, A. S. *Clinical Infectious Diseases* **2001**, *32*, 675-685.

(14) Batt, C. A. *Science (New York, NY)* **2007**, *316*, 1579.

(15) Kirby, B. J.; Jodari, M.; Loftus, M. S.; Gakhar, G.; Pratt, E. D.; Chanel-Vos, C.; Gleghorn, J. P.; Santana, S. M.; Liu, H.; Smith, J. P.; Navarro, V. N.; Tagawa, S. T.; Bander, N. H.; Nanus, D. M.; Giannakakou, P. *PloS one* **2012**, *7*, e35976.

(16) Maheswaran, S.; Haber, D. A. *Current opinion in genetics & development* **2010**, *20*, 96-99.

(17) Zieglschmid, V.; Hollmann, C.; Böcher, O. *Critical reviews in clinical laboratory sciences* **2005**, *42*, 155-196.

(18) Racila, E.; Euhus, D.; Weiss, A. J.; Rao, C.; McConnell, J.; Terstappen, L. W.; Uhr, J. W. *Proceedings of the National Academy of Sciences* **1998**, *95*, 4589-4594.

(19) Wu, J.; Fu, Z. F.; Yan, F.; Ju, H. X. *Trac-Trend Anal Chem* **2007**, *26*, 679-688.

(20) Spisak, S.; Tulassay, Z.; Molnar, B.; Guttman, A. *Electrophoresis* **2007**, *28*, 4261-4273.

(21) Sauer, S.; Lange, B. M.; Gobom, J.; Nyarsik, L.; Seitz, H.; Lehrach, H. *Nature Reviews Genetics* **2005**, *6*, 465-476.

(22) Delamarche, E.; Juncker, D.; Schmid, H. *Advanced Materials* **2005**, *17*, 2911-2933.

(23) Mairhofer, J.; Roppert, K.; Ertl, P. *Sensors-Basel* **2009**, *9*, 4804-4823.

(24) Reichmuth, D. S.; Wang, S. K.; Barrett, L. M.; Throckmorton, D. J.; Einfeld, W.; Singh, A. K. *Lab on a Chip* **2008**, *8*, 1319-1324.

(25) Guan, X.; Zhang, H.-j.; Bi, Y.-n.; Zhang, L.; Hao, D.-l. *Biomedical microdevices* **2010**, *12*, 683-691.

(26) Li, Y.; Zhang, C.; Xing, D. *Analytical biochemistry* **2011**, *415*, 87-96.

(27) Harrison, D. J.; Manz, A.; Fan, Z.; Luedi, H.; Widmer, H. M. *Analytical Chemistry* **1992**, *64*, 1926-1932.

(28) Becker, H.; Gärtner, C. *Analytical and bioanalytical chemistry* **2008**, *390*, 89-111.

(29) McDonald, J. C.; Whitesides, G. M. *Accounts of chemical research* **2002**, *35*, 491-499.

(30) Martinez, A. W.; Phillips, S. T.; Whitesides, G. M.; Carrilho, E. *Analytical chemistry* **2009**, *82*, 3-10.

(31) Carrilho, E.; Martinez, A. W.; Whitesides, G. M. *Analytical chemistry* **2009**, *81*, 7091-7095.

(32) Dungchai, W.; Chailapakul, O.; Henry, C. S. *Analytical chemistry* **2009**, *81*, 5821-5826.

(33) Martinez, A. W.; Phillips, S. T.; Carrilho, E.; Thomas III, S. W.; Sindi, H.; Whitesides, G. M. *Analytical Chemistry* **2008**, *80*, 3699-3707.

(34) Li, X.; Tian, J.; Nguyen, T.; Shen, W. *Analytical chemistry* **2008**, *80*, 9131-9134.

(35) Zhou, G.; Mao, X.; Juncker, D. *Analytical chemistry* **2012**, *84*, 7736-7743.

(36) Saiki, R. K.; Scharf, S.; Faloona, F.; Mullis, K. B.; Horn, G. T.; Erlich, H. A.; Arnheim, N. *Science* **1985**, *230*, 1350-1354.

(37) Cheng, C.-M.; Van, K. T.; Lin, W.; Ruby, R. M. *Journal of Food Protection®* **2009**, *72*, 945-951.

(38) McGuinness, S.; McCabe, E.; O'Regan, E.; Dolan, A.; Duffy, G.; Burgess, C.; Fanning, S.; Barry, T.; O'Grady, J. *Meat science* **2009**, *83*, 555-562.

(39) Hein, I.; Flekna, G.; Krassnig, M.; Wagner, M. *Journal of microbiological methods* **2006**, *66*, 538-547.

(40) Rodriguez-Manzano, J.; Miagostovich, M.; Hundesa, A.; Clemente-Casares, P.; Carratala, A.; Buti, M.; Jardi, R.; Girones, R. *Journal of water and health* **2010**, *8*, 346-354.

(41) Wilding, P.; Shoffner, M. A.; Kricka, L. J. *Clin Chem* **1994**, *40*, 1815-1818.

(42) Wang, J. H.; Chien, L. J.; Hsieh, T. M.; Luo, C. H.; Chou, W. P.; Chen, P. H.; Chen, P. J.; Lee, D. S.; Lee, G. B. *Sensor Actuat B-Chem* **2009**, *141*, 329-337.

(43) Nie, J.; Zhao, Y.; Liu, Y.; Liu, K.; Peng, N. In *Universal Access in Human-Computer Interaction. Context Diversity*, Stephanidis, C., Ed.; Springer Berlin Heidelberg, 2011, pp 398-404.

(44) Xiang, Q.; Xu, B.; Fu, R.; Li, D. *Biomedical Microdevices* **2005**, *7*, 273-279.

(45) Lien, K. Y.; Lee, W. C.; Lei, H. Y.; Lee, G. B. *Biosens Bioelectron* **2007**, *22*, 1739-1748.

(46) Chang, Y.-H.; Lee, G.-B.; Huang, F.-C.; Chen, Y.-Y.; Lin, J.-L. *Biomedical microdevices* **2006**, *8*, 215-225.

(47) Jebrail, M. J.; Wheeler, A. R. *Current opinion in chemical biology* **2010**, *14*, 574-581.

(48) Sista, R.; Hua, Z.; Thwar, P.; Sudarsan, A.; Srinivasan, V.; Eckhardt, A.; Pollack, M.; Pamula, V. *Lab on a Chip* **2008**, *8*, 2091-2104.

(49) Hua, Z.; Rouse, J. L.; Eckhardt, A. E.; Srinivasan, V.; Pamula, V. K.; Schell, W. A.; Benton, J. L.; Mitchell, T. G.; Pollack, M. G. *Analytical chemistry* **2010**, *82*, 2310-2316.

(50) Pratt, E. D.; Huang, C.; Hawkins, B. G.; Gleghorn, J. P.; Kirby, B. J. *Chemical engineering science* **2011**, *66*, 1508-1522.

(51) Gubala, V.; Harris, L. F.; Ricco, A. J.; Tan, M. X.; Williams, D. E. *Analytical Chemistry* **2012**, *84*, 487-515.

(52) Toner, M.; Irimia, D. *Annual review of biomedical engineering* **2005**, *7*, 77.

(53) Chin, C. D.; Linder, V.; Sia, S. K. *Lab on a Chip* **2007**, *7*, 41-57.

(54) Smith, J. P.; Barbati, A. C.; Santana, S. M.; Gleghorn, J. P.; Kirby, B. J. *Electrophoresis* **2012**, *33*, 3133-3142.

(55) Cheng, X.; Irimia, D.; Dixon, M.; Sekine, K.; Demirci, U.; Zamir, L.; Tompkins, R. G.; Rodriguez, W.; Toner, M. *Lab on a Chip* **2007**, *7*, 170-178.

(56) Nagrath, S.; Sequist, L. V.; Maheswaran, S.; Bell, D. W.; Irimia, D.; Ulkus, L.; Smith, M. R.; Kwak, E. L.; Digumarthy, S.; Muzikansky, A.; Ryan, P.; Balis, U. J.; Tompkins, R. G.; Haber, D. A.; Toner, M. *Nature* **2007**, *450*, 1235-1239.

(57) Talasaz, A. H.; Powell, A. A.; Huber, D. E.; Berbee, J. G.; Roh, K.-H.; Yu, W.; Xiao, W.; Davis, M. M.; Pease, R. F.; Mindrinos, M. N. *Proceedings of the National Academy of Sciences* **2009**, *106*, 3970-3975.

(58) Nagrath, S.; Sequist, L. V.; Maheswaran, S.; Bell, D. W.; Irimia, D.; Ulkus, L.; Smith, M. R.; Kwak, E. L.; Digumarthy, S.; Muzikansky, A. *Nature* **2007**, *450*, 1235-1239.

(59) Scheerlinck, J.-P. Y.; Greenwood, D. L. *Drug discovery today* **2008**, *13*, 882-887.

(60) Zeng, Y.; Harrison, D. J. *Analytical Chemistry* **2007**, *79*, 2289-2295.

(61) Velev, O. D.; Lenhoff, A. M. *Current opinion in colloid & interface science* **2000**, *5*, 56-63.

(62) Vlasov, Y. A.; Bo, X.-Z.; Sturm, J. C.; Norris, D. J. *Nature* **2001**, *414*, 289-293.

(63) Reese, C. E.; Asher, S. A. *Analytical chemistry* **2003**, *75*, 3915-3918.

(64) Nazemifard, N.; Bhattacharjee, S.; Masliyah, J. H.; Harrison, D. J. *Angew Chem Int Edit* **2010**, *49*, 3326-3329.

(65) Nazemifard, N.; Bhattacharjee, S.; Masliyah, J. H.; Harrison, D. J. *ELECTROPHORESIS* **2013**, *34*, 2453-2463.

(66) Zeng, Y.; He, M.; Harrison, D. J. *Angewandte Chemie* **2008**, *120*, 6488-6491.

(67) Chang, C. C.; Yang, R. J. *Microfluidics and Nanofluidics* **2007**, *3*, 501-525.

(68) Iverson, B. D.; Garimella, S. V. *Microfluidics and Nanofluidics* **2008**, *5*, 145-174.

(69) Cui, Q. F.; Liu, C. L.; Zha, X. F. *Microfluidics and Nanofluidics* **2007**, *3*, 377-390.

(70) Izzo, I.; Accoto, D.; Menciassi, A.; Schmitt, L.; Dario, P. *Sensor Actuat a-Phys* **2007**, *133*, 128-140.

(71) Tracey, M. C.; Johnston, I. D.; Davis, J. B.; Tan, C. K. L. *Journal of Micromechanics and Microengineering* **2006**, *16*, 1444-1452.

(72) Nguyen, T. T.; Goo, N. S. *Key Eng Mat* **2006**, *326-328*, 245-248.

(73) Chen, S. C.; Cheng, C. H.; Lin, Y. C. *Sensor Actuat a-Phys* **2007**, *135*, 1-9.

(74) Yamahata, C.; Lacharme, F.; Burri, Y.; Gijs, M. A. M. *Sensor Actuat B-Chem* **2005**, *110*, 1-7.

(75) Suzuki, H. *J Intel Mat Syst Str* **2006**, *17*, 1091-1097.

(76) Jeong, O. C.; Park, S. W.; Yang, S. S. *J Mech Sci Technol* **2005**, *19*, 649-654.

(77) Zengerle, R.; Richter, A.; Sandmaier, H. *Ieee Micro Electro Mechanical Systems : An Investigation of Micro Structures, Sensors, Actuators, Machines and Robots* **1992**, 19-24.

(78) Astle, A. A.; Kim, H. S.; Bernal, L. P.; Najafi, K.; Washabaugh, P. D. *Sensor Actuat a-Phys* **2007**, *134*, 245-256.

(79) Chang, H. T.; Lee, C. Y.; Wen, C. Y. *Microsyst Technol* **2007**, *13*, 1615-1622.

(80) Sim, W.; Oh, J.; Choi, B. *Microsyst Technol* **2006**, *12*, 1085-1091.

(81) Kim, J. H.; Na, K. H.; Kang, C. J.; Kim, Y. S. *Sensor Actuat a-Phys* **2005**, *120*, 365-369.

(82) Shin, D. D.; Mohanchandra, K. R.; Carman, G. P. *Sensor Actuat a-Phys* **2005**, *119*, 151-156.

(83) Inman, W.; Domansky, K.; Serdy, J.; Owens, B.; Trumper, D.; Griffith, L. G. *Journal of Micromechanics and Microengineering* **2007**, *17*, 891-899.

(84) Xu, T. B.; Su, J. *Sensor Actuat a-Phys* **2005**, *121*, 267-274.

(85) Lee, S.; Kim, K. J.; Park, H. C. *Smart Structures and Materials 2005: Electroactive Polymer Actuators and Devices( EAPAD)* **2005**, *5759*, 439-446.

(86) Good, B. T.; Bowman, C. N.; Davis, R. H. *J Colloid Interf Sci* **2007**, *305*, 239-249.

(87) Lin, Q.; Yang, B. Z.; Xie, J.; Tai, Y. C. *Journal of Micromechanics and Microengineering* **2007**, *17*, 220-228.

(88) Goulpeau, J.; Trouchet, D.; Ajdari, A.; Tabeling, P. *J Appl Phys* **2005**, *98*.

(89) Samel, B.; Griss, P.; Stemme, G. *J Microelectromech S* **2007**, *16*, 50-57.

(90) Yamahata, C.; Chastellain, M.; Parashar, V. K.; Petri, A.; Hofmann, H.; Gijs, M. A. M. *J Microelectromech S* **2005**, *14*, 96-102.

(91) Jung, J. Y.; Kwak, H. Y. *Microfluidics and Nanofluidics* **2007**, *3*, 161-169.

(92) Yin, Z. Z.; Prosperetti, A. *Journal of Micromechanics and Microengineering* **2005**, *15*, 1683-1691.

(93) Eddings, M. A.; Gale, B. K. *Journal of Micromechanics and Microengineering* **2006**, *16*, 2396-2402.

(94) Song, W. H.; Lichtenberg, J. *Journal of Micromechanics and Microengineering* **2005**, *15*, 1425-1432.

(95) Matteucci, M.; Perennes, F.; Marmiroli, B.; Miotti, P.; Vaccari, L.; Gosparini, A.; Turchet, A.; Di Fabrizio, E. *Microelectron Eng* **2006**, *83*, 1288-1290.

(96) Lei, K. F.; Law, W. C.; Suen, Y. K.; Li, W. J.; Yam, Y.; Ho, H. P.; Kong, S. K. *P I Mech Eng H* **2007**, *221*, 129-141.

(97) Abdelgawad, M.; Hassan, I.; Esmail, N.; Phutthavong, P. *J Fluid Eng-T Asme* **2005**, *127*, 734-742.

(98) Yokota, K.; Sato, K.; Itoh, M. *Jsme Int J B-Fluid T* **2006**, *49*, 393-400.

(99) Felten, M.; Geggier, P.; Jager, M.; Duschl, C. *Phys Fluids* **2006**, *18*.

(100) Singhal, V.; Garimella, S. V. *Sensor Actuat a-Phys* **2007**, *134*, 650-659.

(101) Darabi, J.; Wang, H. X. *J Microelectromech S* **2005**, *14*, 747-755.

(102) Go, D. B.; Garimella, S. V.; Fisher, T. S.; Mongia, R. K. *J Appl Phys* **2007**, *102*.

(103) Lin, C. W.; Jang, J. Y. *Sensor Actuat a-Phys* **2005**, *122*, 167-176.

(104) Darabi, J.; Rada, M.; Ohadi, M.; Lawler, J. *J Microelectromech S* **2002**, *11*, 684-690.

(105) Chen, Z.; Wang, P.; Chang, H.-C. *Analytical and bioanalytical chemistry* **2005**, *382*, 817-824.

(106) Debesset, S.; Hayden, C.; Dalton, C.; Eijkel, J.; Manz, A. *Lab on a Chip* **2004**, *4*, 396-400.

(107) Mpholo, M.; Smith, C.; Brown, A. *Sensors and Actuators B: Chemical* **2003**, *92*, 262-268.

(108) Homsy, A.; Linder, V.; Lucklum, F.; De Rooij, N. *Sensors and Actuators B: Chemical* **2007**, *123*, 636-646.

(109) Bahadur, V.; Garimella, S. V. *Journal of Micromechanics and Microengineering* **2006**, *16*, 1494-1503.

(110) Bahadur, V.; Garimella, S. V. *Langmuir* **2007**, *23*, 4918-4924.

(111) Nakano, M.; Katsura, S.; Touchard, G. G.; Takashima, K.; Mizuno, A. *Ieee T Ind Appl* **2007**, *43*, 232-237.

(112) Nguyen, N. T.; Meng, A. H.; Black, J.; White, R. M. *Sensor Actuat a-Phys* **2000**, *79*, 115-121.

(113) Chin, C. D.; Laksanasopin, T.; Cheung, Y. K.; Steinmiller, D.; Linder, V.; Parsa, H.; Wang, J.; Moore, H.; Rouse, R.; Umviligihozo, G. *Nature medicine* **2011**, *17*, 1015-1019.

(114) Chin, C. D.; Laksanasopin, T.; Cheung, Y. K.; Steinmiller, D.; Linder, V.; Parsa, H.; Wang, J.; Moore, H.; Rouse, R.; Umviligihozo, G.; Karita, E.; Mwambarangwe, L.; Braunstein, S. L.; van de Wijgert, J.; Sahabo, R.; Justman, J. E.; El-Sadr, W.; Sia, S. K. *Nature medicine* **2011**, *17*, 1015-1019.

(115) Barz, D. P. J.; Ehrhard, P. *Lab on a Chip* **2005**, *5*, 949-958.

(116) McCreedy, T. *TrAC Trends in Analytical Chemistry* **2000**, *19*, 396-401.

(117) Bromberg, A.; Mathies, R. A. *Electrophoresis* **2004**, *25*, 1895-1900.

(118) Rodriguez-Mozaz, S.; Reder, S.; de Alda, M. L.; Gauglitz, G.; Barcelo, D. *Biosens Bioelectron* **2004**, *19*, 633-640.

(119) Yadavalli, V. K.; Pishko, M. V. *Anal Chim Acta* **2004**, *507*, 123-128.

(120) Phillips, T. M. *Electrophoresis* **2004**, *25*, 1652-1659.

(121) Wang, J.; Ahmad, H.; Ma, C.; Shi, Q.; Vermesh, O.; Vermesh, U.; Heath, J. *Lab on a Chip* **2010**, *10*, 3157-3162.

(122) Fan, R.; Vermesh, O.; Srivastava, A.; Yen, B. K.; Qin, L.; Ahmad, H.; Kwong, G. A.; Liu, C.-C.; Gould, J.; Hood, L. *Nature biotechnology* **2008**, *26*, 1373-1378.

(123) Ikami, M.; Kawakami, A.; Kakuta, M.; Okamoto, Y.; Kaji, N.; Tokeshi, M.; Baba, Y. *Lab on a Chip* **2010**, *10*, 3335-3340.

(124) Kim, S. H.; Shim, J. W.; Yang, S. M. *Angewandte Chemie* **2011**, *123*, 1203-1206.

(125) Appleyard, D. C.; Chapin, S. C.; Doyle, P. S. *Analytical chemistry* **2010**, *83*, 193-199.

(126) Kang, Q. S.; Shen, X. F.; Hu, N. N.; Hu, M. J.; Liao, H.; Wang, H. Z.; He, Z. K.; Huang, W. H. *Analyst* **2013**, *138*, 2613-2619.

(127) Connelly, J. T.; Kondapalli, S.; Skoupi, M.; Parker, J. S.; Kirby, B. J.; Baeumner, A. J. *Analytical and bioanalytical chemistry* **2012**, *402*, 315-323.

(128) Chen, G. D.; Alberts, C. J.; Rodriguez, W.; Toner, M. *Analytical chemistry* **2009**, *82*, 723-728.

(129) Gijs, M. A.; Lacharme, F.; Lehmann, U. *Chemical reviews* **2009**, *110*, 1518-1563.

(130) Teste, B.; Malloggi, F.; Siaugue, J.-M.; Varenne, A.; Kanoufi, F.; Descroix, S. *Lab on a Chip* **2011**, *11*, 4207-4213.

(131) Liu, Y.; Yang, D.; Yu, T.; Jiang, X. *Electrophoresis* **2009**, *30*, 3269-3275.

(132) Connelly, J. T.; Kondapalli, S.; Skoupi, M.; Parker, J. S.; Kirby, B. J.; Baeumner, A. J. *Analytical and bioanalytical chemistry* **2012**, *402*, 315-323.

(133) Rubina, A. Y.; Filippova, M.; Feizkhanova, G.; Shepeliakovskaya, A.; Sidina, E.; Boziev, K. M.; Laman, A.; Brovko, F.; Vertiev, Y. V.; Zasedatelev, A. *Analytical chemistry* **2010**, *82*, 8881-8889.

(134) Appleyard, D. C.; Chapin, S. C.; Srinivas, R. L.; Doyle, P. S. *Nature protocols* **2011**, *6*, 1761-1774.

(135) Wakayama, H.; Henares, T. G.; Jigawa, K.; Funano, S.-i.; Sueyoshi, K.; Endo, T.; Hisamoto, H. *Lab Chip* **2013**, *13*, 4304-4307.

(136) Son, K. J.; Shin, D.-S.; Kwa, T.; Gao, Y.; Revzin, A. *Analytical chemistry* **2013**, *85*, 11893-11901.

(137) Malekpourkoupaei, A.; Kostiuk, L. W.; Harrison, D. J. *Chemistry of Materials* **2013**, *25*, 3808-3815.

(138) Ceriotti, L.; de Rooij, N. F.; Verpoorte, E. *Analytical chemistry* **2002**, *74*, 639-647.

(139) Adam, T.; Unger, K. K.; Dittmann, M. M.; Rozing, G. P. *Journal of Chromatography A* **2000**, *887*, 327-337.

(140) Araz, M. K.; Tentori, A. M.; Herr, A. E. *Journal of laboratory automation* **2013**, 2211068213491408.

(141) Berry, S. M.; Alarid, E. T.; Beebe, D. J. *Lab on a chip* **2011**, *11*, 1747-1753.

(142) McKenna, B. K.; Evans, J. G.; Cheung, M. C.; Ehrlich, D. J. *Nature methods* **2011**, *8*, 401-403.

(143) Ng, A. H.; Choi, K.; Luoma, R. P.; Robinson, J. M.; Wheeler, A. R. *Analytical chemistry* **2012**, *84*, 8805-8812.

(144) Bogojevic, D.; Chamberlain, M. D.; Barbulovic-Nad, I.; Wheeler, A. R. *Lab on a Chip* **2012**, *12*, 627-634.